AD-A089 179 DAEDALEAN ASSOCIATES INC WOODBINE MD F/G 13/8
EXPERIMENTAL RESEARCH ON THE MECHANISMS OF FORMATION FOR SPHERO--ETC(U)
AUG 80 S E HICKMAN, T J STANSFIELD N00014-77-C-0648
UNCLASSIFIED DAI-TJS-7775-001-TR NL

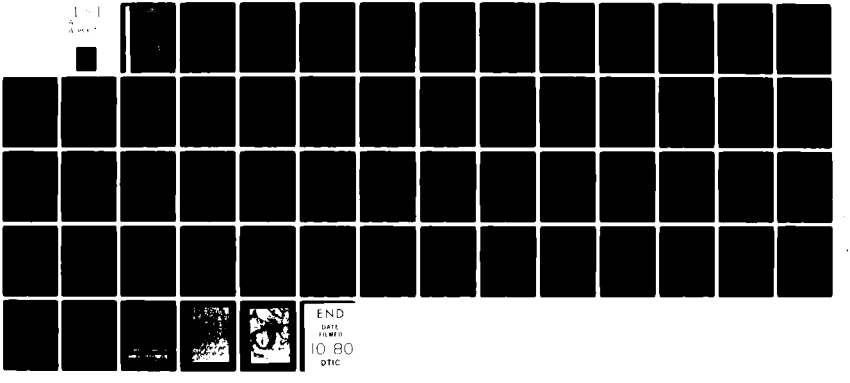

END
DATE FILMED
10-80
DTIC

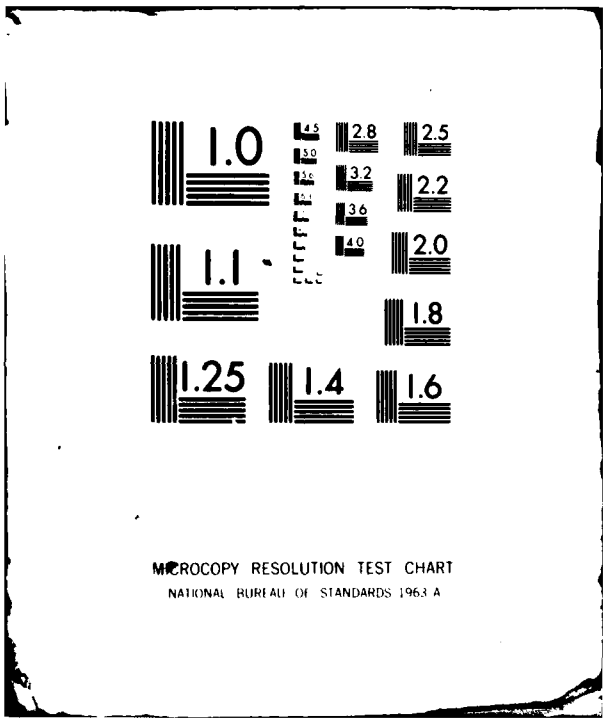
1.0
1.1
1.25
1.4
1.6
1.8
2.0
2.2
2.5
2.8
3.2
3.6
4.0
4.5
5.0
MICROCOPY RESOLUTION TEST CHART
NATIONAL BUREAU OF STANDARDS 1963 A

LEVEL II

12

DAEDALEAN ASSOCIATES, INC.

ENGINEERING, DESIGN AND ANALYSIS SERVICES

AD A089179

DTIC
ELECTE
SEP 1 2 1980
S
E

DDC FILE COPY

DAI

DISTRIBUTION STATEMENT A
Approved for public release;
Distribution Unlimited

SPRINGLAKE RESEARCH CENTER
15110 FREDERICK ROAD
WOODBINE, MARYLAND 21797

80 8 15 026

DAEDALEAN ASSOCIATES, Incorporated

LEVEL II

(9) TECHNICAL REPORT

(6) EXPERIMENTAL RESEARCH ON THE MECHANISMS OF FORMATION FOR SPHEROIDS PRODUCED BY CAVITATION EROSION.

Submitted to:

Office of Naval Research
Fluid Dynamics Program
Code 438
Department of the Navy
800 North Quincy Street
Arlington, VA 22217

By

(10) Scott E. Hickman
Thomas J. Stansfield
Stephen C. Howard
and
William H. Bohli

DTIC
ELECTE
SEP 12 1980
S D
E

(15) N00014-77-C-[illegible]

The views and conclusions contained in this document are those of the authors and should not be interpreted as necessarily representing the official policies, either expressed or implied, of the U. S. Navy or of the U. S. Government.

(14) DAI Technical Report
DAI-TJS-7775-001-TR

(12) 58

(11) Aug[redacted]80

DISTRIBUTION STATEMENT A
Approved for public release;
Distribution Unlimited

390 155

ACKNOWLEDGMENTS

This work was performed under the auspices of the Fluid Dynamics Program of the Office of Naval Research (Department of the Navy) under Contract No. N00014-77-C-0648. LCDR Hal Martin was the Technical Monitor of the program.

Accession For
NTIS GRA&I ☑
DDC TAB ☐
Unannounced ☐
Justification PER LETTER ON FILE
By
Distribution/
Availability Codes
Dist. | Avail and/or special
A

TABLE OF CONTENTS

	Page
ACKNOWLEDGMENTS	i
LIST OF FIGURES	iv
1.0 INTRODUCTION	1
1.1 Background	1
2.0 EXPERIMENTAL APPARATUS, TECHNIQUES, AND PROCEDURES	3
2.1 Erosion of Test Specimens Utilizing the Standard ASTM Vibratory Apparatus	3
2.1.1 Test Materials and Liquid Test Media	4
2.1.2 Lead Specimen Mounting Technique	4
2.1.3 Particle Collection Technique	5
2.2 Erosion of Test Specimen Using CONCAVER™ System	6
3.0 DISCUSSION OF EXPERIMENTAL RESULTS	9
3.1 Erosion of Monel	9
3.1.1 Particle Analysis of Monel Eroded in Distilled Water	9
3.1.2 Particle Analysis of Monel Eroded in 10W Oil	10
3.1.3 Comparison of Monel Tests	11

Page

3.2 Erosion of Lead 11

3.2.1 Particle Analysis of Lead Eroded in Distilled Water 11

3.2.2 Particle Analysis of Lead Eroded in 10W Oil 12

3.2.3 Comparison of Results of Lead Tests . . 12

3.3 Particle Analysis of Aluminum Eroded in 10W Oil 13

3.4 Particle Analysis of Nickel Eroded in Distilled Water 13

3.5 Comparative Analysis of Spherical Particles Generated from the Four Specimen Materials 14

3.6 Analysis of Erosion Particles Produced by the CONCAVER System 14

4.0 CONCLUSIONS AND RECOMMENDATIONS 16

4.1 Conclusions 16

4.2 Recommendations 17

REFERENCES 18

LIST OF FIGURES

FIGURE 1 - ASTM STANDARD VIBRATORY APPARATUS

FIGURE 2 - MODIFIED ALUMINUM BUTTON WITH LEAD PLATE ATTACHED

FIGURE 3 - VIBRATORY TEST APPARATUS USED TO ERODE 1/8 INCH LEAD SPECIMEN PLATE

FIGURE 4 - LEAD SPECIMEN THAT WAS ERODED IN DISTILLED WATER BY TITANIUM BUTTON

FIGURE 5 - METALLURGICAL MICROSCOPE USED TO MEASURE PARTICLE DIAMETERS

FIGURE 6 - TRIPLEX PLUNGER PUMP AND MOTOR COMBINATION CAPABLE OF 5 GPM AT 20,000 PSI

FIGURE 7 - PARTICLE COLLECTION CHAMBER

FIGURE 8 - SKETCH OF EDGERTON'S HIGH SPEED PHOTOGRAPH OF A MILKDROP ILLUSTRATING THE SPLASH-SPRAY THEORETICAL RESULT

FIGURE 9 - PARTICLE SIZE DISTRIBUTION CURVE FOR MONEL SPHERICAL PARTICLES GENERATED FROM EROSION IN DISTILLED WATER

FIGURE 10 - PHOTOMICROGRAPH OF A 13μ LONG 3μ WIDE MONEL ROD WITH TWO 6μ SPHERICAL PARTICLES LOCATED DIRECTLY BELOW

FIGURE 11 - SCANNING ELECTRON PHOTOMICROGRAPH OF MONEL PARTICLES GENERATED FROM EROSION IN DISTILLED WATER

FIGURE 12 - SCANNING ELECTRON PHOTOMICROGRAPH OF TWO MONEL SPHERICAL PARTICLES GENERATED FROM EROSION IN DISTILLED WATER

FIGURE 13 - SCANNING ELECTRON PHOTOMICROGRAPH OF AN 11μ MONEL SPHERICAL PARTICLE GENERATED FROM EROSION IN DISTILLED WATER

FIGURE 14 - SCANNING ELECTRON PHOTOMICROGRAPH OF AN 8μ MONEL SPHERICAL PARTICLE GENERATED FROM EROSION IN DISTILLED WATER

FIGURE 15 - SCANNING ELECTRON PHOTOMICROGRAPH OF A 6μ MONEL SPHERICAL PARTICLE GENERATED FROM EROSION IN DISTILLED WATER SHOWING CRATERLIKE INDENTATION

FIGURE 16 - SCANNING ELECTRON PHOTOMICROGRAPH OF A 12μ LONG, 4μ DIAMETER CYLINDRICAL MONEL ROD GENERATED FROM EROSION IN DISTILLED WATER

FIGURE 17 - PARTICLE SIZE DISTRIBUTION CURVE FOR MONEL SPHERICAL PARTICLES GENERATED FROM EROSION IN 10W OIL

FIGURE 18 - SCANNING ELECTRON PHOTOMICROGRAPH OF A 10μ MONEL SPHERICAL PARTICLE GENERATED FROM EROSION IN 10W OIL

FIGURE 19 - PARTICLE SIZE HISTOGRAM FOR LEAD SPHERICAL PARTICLES GENERATED FROM EROSION IN DISTILLED WATER

FIGURE 20 - SCANNING ELECTRON PHOTOMICROGRAPH OF A 40μ LEAD SPHEROID GENERATED FROM EROSION IN DISTILLED WATER

FIGURE 21 - SCANNING ELECTRON PHOTOMICROGRAPH OF A LEAD, ROD SHAPED PARTICLE 257μ LONG AND 123μ IN DIAMETER GENERATED FROM EROSION IN DISTILLED WATER

FIGURE 22 - PARTICLE SIZE HISTOGRAM FOR LEAD SPHERICAL PARTICLES GENERATED FROM EROSION IN 10W OIL

FIGURE 23 - SCANNING ELECTRON PHOTOMICROGRAPH OF A 390μ LEAD SPHEROID, REVEALING SURFACE ABRASIONS, GENERATED FROM EROSION IN 10W OIL

FIGURE 24 - SCANNING ELECTRON PHOTOMICROGRAPH OF A ROD SHAPED, LEAD PARTICLE 375μ LONG AND 70μ IN DIAMETER

FIGURE 25 - SCANNING ELECTRON PHOTOMICROGRAPH OF A 35μ LEAD SPHEROID SOLIDIFIED DURING FORMATION

FIGURE 26 - PARTICLE SIZE DISTRIBUTION CURVE FOR ALUMINUM SPHERICAL PARTICLES GENERATED FROM EROSION IN 10W OIL

FIGURE 27 - SCANNING ELECTRON PHOTOMICROGRAPH OF A 65μ ALUMINUM SPHEROID GENERATED FROM EROSION IN 10W OIL

FIGURE 28 - SCANNING ELECTRON PHOTOMICROGRAPHIC CLOSE-UP OF THE SPHERE DEPICTED IN FIGURE 27 SHOWING THE POINT OF CONNECTION BETWEEN SPHERE AND ROD

FIGURE 29 - PARTICLE SIZE DISTRIBUTION CURVE FOR NICKEL SPHERICAL PARTICLES GENERATED FROM EROSION IN DISTILLED WATER

FIGURE 30 - SCANNING ELECTRON PHOTOMICROGRAPH OF AN 8μ NICKEL SPHERICAL PARTICLE GENERATED FROM EROSION IN DISTILLED WATER

FIGURE 31 - SCANNING ELECTRON PHOTOMICROGRAPH OF A 28μ LONG, 6μ DIAMETER, NICKEL ROD IN CLOSE PROXIMITY TO A 7μ NICKEL SPHEROID

FIGURE 32 - SCANNING ELECTRON PHOTOMICROGRAPH OF THE ERODED FACE OF THE NICKEL VIBRATORY BUTTON SHOWING PLASTIC DEFORMATION

FIGURE 33 - SCANNING ELECTRON PHOTOMICROSCOPIC CLOSE-UP OF THE NICKEL VIBRATORY BUTTON FROM FIGURE 32 SHOWING A 9μ CONCAVE CRATER

EXPERIMENTAL RESEARCH ON THE MECHANISMS OF FORMATION FOR SPHEROIDS PRODUCED BY CAVITATION EROSION

1.0 INTRODUCTION

In modern machinery, a major cause of unscheduled downtime is the wear and eventual failure of load carrying components such as shafts, gears, and bearings. These wear and fatigue failures precipitate wear particles such as metal fragments, shavings, and chips. The mechanisms involved in the formation of wear particles, if understood, would lead to an optimization of the failure prediction method. A potentially important mechanism of wear is the application and release of a local high pressure on a working surface. This wear, known as cavitation erosion, is recognized as a powerfully destructive force in many high speed hydrodynamic systems. Cavitation is one of the major problems confronting designers and users of modern high speed hydrodynamic systems such as pumps, marine propellers, hydraulic turbines, valves and control devices, hydrofoils, sonar domes, other acoustic signal devices, bearings, and diesel engine wet-cylinder liners.(1)*

1.1 Background

Under the initial feasibility study conducted at DAEDALEAN ASSOCIATES, Inc. (DAI), the standard ASTM vibratory cavitation

---

* Numbers in parenthesis refer to references at the end of this Technical Report.

erosion tests were conducted on annealed SAE 52100 bearing steel and 1100-F aluminum. The two test media used were SAE 10W non-detergent lubricating oil and distilled water. Analysis of the eroded particles indicated a large degree of plastic deformation prior to failure.(2) Most of the eroded particles were of irregular shape. However, smooth, perfectly spherical particles, spheroids, were also observed. Spheroids were observed in both oil and distilled water by erosion of 52100 bearing steel, and 1100-F aluminum. It has been theorized that the high strain rates caused by the implosion of the cavity bubbles led to the plastic flow of the metals into the surrounding fluid where surface tension produced spheroids.(3)

To further understand the mechanisms of spherical particle formation, the cavitation erosion particles from three additional specimen materials, nickel, monel, and lead have been studied in the current program.

This report describes the apparatus, techniques, and procedures utilized for generating, collecting, and analyzing spherical cavitation erosion particles. The laboratory results are discussed along with the conclusions and recommendations resulting from the experimental program.

2.0 EXPERIMENTAL APPARATUS, TECHNIQUES, AND PROCEDURES

Several recognized techniques are presently being utilized to conduct cavitation erosion investigations in the laboratory. These include:

1. The ASTM vibratory apparatus;
2. The rotating disk apparatus, and;
3. The liquid jet impact apparatus.

The erosion debris generated from two of these methods, the ASTM vibratory apparatus, and the liquid jet impact apparatus have been analyzed during this program with the emphasis placed upon characterizing spherical erosion particles.

2.1 Erosion of Test Specimens Utilizing the Standard ASTM Vibratory Apparatus

Figure 1 is a photograph of the ASTM vibratory apparatus utilized to generate spherical erosion particles during this program. This equipment consists of a commercially available piezoelectric transducer, velocity transformer, power supply, and voltmeter. The vibratory equipment drives a test specimen through a small amplitude, high frequency, axial oscillation. The oscillation produces alternating pressure fields causing cavitation bubbles to grow and collapse on the specimen's surface. In order to produce the cavitation bubbles, the face of the test specimen must be submerged within a fluid media. The frequency of vibration was fixed at 20 KHz. The peak to peak displacement amplitude was 2×10^{-3} inches. Since heat is a

byproduct of the acoustic energy radiating from the test specimen, a temperature bath was utilized to maintain the various test liquids at a constant temperature of 80°F ± 2°F.

2.1.1 Test Materials and Liquid Test Media

Four specimen materials were eroded using the ASTM vibratory equipment. Aluminum, nickel, monel, and lead samples were eroded in both distilled water and 10W nondetergent oil. The erosion of the sample materials in distilled water took an average time of two hours per specimen to collect a sufficient amount of particles for analysis. The erosion of the sample materials in 10W nondetergent oil required an average time of 30 hours per specimen.

2.1.2 Lead Specimen Mounting Technique

A specimen mounting technique had to be developed in order to erode the lead specimens. The cavitation button attached to the end of the vibratory horn must weigh ten grams in order for the system to vibrate properly. In the case of the lead specimen, the combined weight of the button and the threaded mounting pin was greater than the allowable ten grams. This additional weight increment prevented the system from achieving the specified vibratory mode required to attain cavitation erosion. The first attempt to fabricate a ten gram lead button consisted of securing a three gram piece of lead to a specially machined, seven gram aluminum button with an epoxy glue. Figure 2 is a photograph of this modified aluminum button with the lead tip

attached. This technique was unsuccessful due to the lead having a tendency to separate from the aluminum as a result of the high tensile stresses produced by the frequency of vibration.

Figure 3 depicts the test apparatus used to successfully erode a 1/8 inch lead plate. This technique involved placing a titanium button on the end of the vibratory horn. The lead specimen was suspended in either distilled water or 10W nondetergent oil. The titanium button was then lowered to within 0.025 inches of the surface of the lead plate. The titanium button vibrated causing cavitation erosion to occur on the face of the titanium button. The lead plate was in such close proximity to the titanium button that it was eroded by the cavitation bubbles collapsing upon its surface. The erosion strength of titanium was significantly higher than the erosion strength of lead. In the amount of time used to erode the lead plate, a negligible amount of erosion occurred on the titanium button. Figure 4 is a photograph of the lead sample after it was eroded in distilled water.

2.1.3 Particle Collection Technique

Once the particles had been eroded from the test material, the particles were separated from the test fluid for study. The simplest method for separating the particles from the test fluid was sedimentation. The particles eroded in distilled water settled to the bottom of the beaker within a 24 hour period. The excess water was carefully siphoned away and the erosion

particles were allowed to dry. The particles eroded in 10W non-detergent oil did not settle as quickly through the oil. It was necessary to dilute the oil in order to lower its viscosity so that the particles could settle more quickly. A mixture of one part hexane to one part oil allowed all of the particles to settle within a 48 hour period.

The dried erosion particles were then mounted on specimen plates which could be placed in either a metallurgical microscope or in a scanning electron microscope for examination. This mounting technique insured that the particles which were studied with the metallurgical microscope, shown in Figure 5, would also be the particles photographed by the scanning electron microscope.

Particle size distribution curves were developed for each specimen material. The metallurgical microscope has a scale etched on an eyepiece which was used to measure the particle diameters. The eyepiece scale was calibrated with a 0.011 mm division micro-scale.

2.2 Erosion of Test Specimen Using CONCAVER™ System

Cavitation erosion particles were also generated using a cavitating water jet system. Figure 6 is the pumping system used to eroded aluminum specimen plates. This system is capable of delivering five gallons per minute with a maximum pressure of 20,000 psi.

Figure 7 shows the particle collection chamber used for the collection of particles produced by the cavitation water jet system. The chamber was constructed of 1/2 inch thick Plexiglas. Plexiglas was the chosen tank material to insure that the eroded particles would not be confused with metallic particles from a metal tank wall. Plexiglas also proved to be a good material since it allowed for complete visibility and easy particle detection. A bulkhead fitting was installed in one wall of the chamber to allow the specimen support rod to penetrate the chamber. In this manner the specimen distance and exposed area could be adjusted during particle production. In the opposite wall of the chamber another bulkhead fitting was installed to handle the specially designed supply tube and nozzle. This assembly also allowed the nozzle distance from the specimen to be adjusted. With the CONCAVER™ system, water was pumped at high pressure through a nozzle specifically designed to produce a cavitating water jet which impinged upon the specimen plate thereby eroding particles. The water was discharged through a port in the top of the chamber. The arrangement of the discharge port allowed the particles to settle in the chamber and be collected.

Aluminum specimen plates were eroded using the particle collection chamber. The test conditions used to generate aluminum particles were: 1. a nozzle pressure of 13,000 psi, 2. a nozzle distance of 2 inches, and 3. a nozzle diameter of 0.025 inches. After the particles were generated, they were dried, mounted,

and examined using the technique described in the previous section.

3.0 DISCUSSION OF EXPERIMENTAL RESULTS

The analysis of the erosion particles generated during this program has been accomplished through the use of:

1. metallurigical microscope with photographic capability;
2. scanning electron microscope analysis and photography, and;
3. energy dispersive X-ray analyzer (for particle identification).

The plastic flow of metal due to high speed cavitation bubble collapse can be visualized from an analysis of Edgerton's high speed milkdrop photograph (4) illustrated in Figure 8. This plastic flow, described as one of spherical drops splashing out of a liquid crater and then solidifying, is an accepted theory of the mechanism of spheroid formation. Scanning electron photomicrographs taken of the erosion particles generated during this program show evidence in support of the splash-spray theory.

3.1 Erosion of Monel

3.1.1 Particle Analysis of Monel Eroded in Distilled Water

Figure 9 is the particle size distribution curve for monel spherical particles generated from erosion in distilled water. Approximately 120 spherical particles were observed, with the majority of the spherical particles (43 percent of the total) being 6μ in diameter. Figure 10 is a wide angle photomicrograph

of monel particles. This figure reveals the power capability of the microscope utilized in generating the particle distribution curves that are incorporated into this report. Figure 11 is a scanning electron photomicrograph of the specimen mount containing monel particles. The particles previously counted as perfect spheroids (when viewed on the laboratory microscope) consisted of partially formed, oblong, and plastically deformed spherical particles in addition to perfect spheres. Figures 12, 13, and 14 are scanning electron microscope photographs of the typical shape of spheroid particles found throughout the range of materials analyzed. Figure 15 is a scanning electron photomicrograph of a 6μ diameter spherical particle with a concaver crater-like deformation. Figure 16 is a scanning electron photomicrograph of a 12μ long, 4μ diameter cylindrical rod identified as monel.

3.1.2 Particle Analysis of Monel Eroded in 10W Oil

Figure 17 is the particle distribution curve for monel spherical particles generated from erosion in 10W nondetergent oil. Approximately 120 spheres were observed, with the majority of the spheres (32 percent of the total) being 3μ in diameter. The total time for the test cycle of eroding monel in 10W oil was 34.25 hours. Figure 18 is a scanning electron photomicrograph of a 10μ monel spheroid. This particle lacks the smooth surface property found in the analysis of the monel/water combination.

3.1.3 Comparison of Monel Tests

The physical appearance between the monel particles generated in oil and in water was very similar. Upon close examination of the particles, it was observed that the particles produced by the erosion of the material in water were smoother in surface texture than the particles produced in the oil medium. The particles generated by erosion in oil had a slight "orange peel" texture.

In the water medium tests, the largest number of particles occurred at a particle size of 6μ. This size accounted for 43 percent of the total number of particles produced. The group of particles smaller than 6μ accounted for 21 percent of the total. The remaining group of particles, those above 6μ, contained 36 percent of the total number of particles.

The greatest number of particles produced in oil occurred at a smaller particle size, 3μ, than the size of the most numerous particles produced in water. The 3μ particles produced in oil accounted for 32 percent of the total. Forty-nine percent of the particles were greater in size than 3μ and 19 percent of the particles were less than 3μ.

3.2 Erosion of Lead

3.2.1 Particle Analysis of Lead Eroded in Distilled Water

Figure 19 is the particle size histogram for lead spherical particles generated from erosion in distilled water. Approximately 70 spheres were observed with the majority of the spheres

(63 percent of the total) ranging in diameter from 100μ to 200μ. Figure 20 is a scanning electron photomicrograph of a 40μ diameter lead spheriod. Figure 21 is a scanning electron photomicrograph of a lead, rod shaped, particle 257μ long and 123μ in diameter. A lateral crack, located to the right of center of the rod, suggests that this is a spheroid solidified during the process of separation.

3.2.2 Particle Analysis of Lead Eroded in 10W Oil

Figure 22 is the particle size histogram for lead spherical particles generated from erosion in 10W nondetergent oil. Approximately 47 spheres were observed with the majority of the spheres (49 percent of the total) ranging in diameter from 80μ to 170μ. The lead particles analyzed were considerably larger than the other particles analyzed. Figure 23 is a scanning electron photomicrograph of a 390μ lead sphere. This particle has surface abrasions caused by the effects of formation. Figure 24 is a scanning electron photomicrograph of a rod-shaped lead particle 350μ long and 70μ in diameter. Figure 25 is a scanning electron photomicrograph of a 35μ lead spherical particle solidified during formation.

3.2.3 Comparison of Results of Lead Tests

The physical appearance of the particles generated in oil and water was very similar. They all exhibited rather rough surfaces and surface abrasions were quite evident.

The particle size distributions for particles eroded in both the oil and water media was also similar. In both cases, the

110μ size graph contained the greatest number of particles.

3.3 Particle Analysis of Aluminum Eroded in 10W Oil

Figure 26 is the particle distribution curve for aluminum spherical particles generated from erosion in 10W nondetergent oil. Approximately 70 spheres were observed, with the majority of the spheres (31 percent of the total) being 6μ in diameter. Figure 27 is a scanning electron photomicrograph of a 65μ diameter aluminum spheroid. It should be observed in this photo that the sphere is connected to a rod shaped particle. Closer examination, Figure 28, reveals that the particle is indeed attached to the rod. The length of the contact point is 9μ. Plastic deformation along the edge of the rod is evident.

3.4 Particle Analysis of Nickel Eroded in Distilled Water

Figure 29 is the particle size distribution curve for nickel spherical particles generated from erosion in distilled water. Approximately 100 spheres were observed with the majority of the spheres (42 percent of the total) being 5μ in diameter. Figure 30 is a scanning electron photomicrograph of an 8μ diameter nickel spherical particle. This sphere, surrounded by irregularly shaped erosion debris, has one flat side. Figure 31 is a scanning electron photomicrograph of a 7μ diameter spherical particle. Figure 32 is a scanning electron photomicrograph of the nickel button eroded in distilled water. The face of this button is pitted and cratered. Figure 33 is a scanning electron photomicrographic close-up of the nickel button of Figure 32. The crater shown is 9μ in diameter. The edges of this and other

craters viewed on this button reveal the kind of melted texture that would accompany the plastic flow produced by extremely high rates of deformation and associated high localized temperatures.

3.5 Comparative Analysis of Spherical Particles Generated from the Four Specimen Materials

Spherical erosion particles were produced from all four specimen materials. The spheroid particles produced in monel, aluminum and nickel all averaged a particle diameter of 5μ. The spherical particles from these materials ranged in size between 1μ and 20μ. The lead spheres, produced by the method described in Section 2.1.2, were much larger. The lead spheres ranged in size from 60μ to 360μ in diameter. The majority of the lead spheres were between 100μ and 200μ in diameter.

3.6 Analysis of Erosion Particles Produced by the CONCAVER System

Aluminum test samples were eroded using a cavitating water jet. The erosion particles were examined and very few spherical particles were found. Many of the irregularly shaped particles had rounded, smooth edges. However, there were not many perfect spheres.

One of the problems involved with examination of erosion debris produced with a cavitating water jet is the separation of the particles from the water. Large quantities of water are used to produce a small number of particles. In 10 gallons of water there will be less than 0.5 grams of eroded material.

Filter paper will separate the particles from the water, but the particles are then trapped in the filter paper. For future tests, a centrifuge could be utilized to separate the small amount of particles from the large amounts of water.

4.0 CONCLUSIONS AND RECOMMENDATIONS

The successful completion of the tasks of this program has yielded sufficient engineering data to justify the following conclusions and recommendations.

4.1 Conclusions

1. The spheroid particles produced in monel, aluminum, and nickel all averaged a mean diameter of 5μ. The spherical particles from these materials all ranged in size between 1μ and 20μ.
2. The particles resulting from erosion in the 10W nondetergent oil, on an average, took 15 times longer to generate than did the particles produced from erosion in distilled water.
3. Testing utilizing the CONCAVER system to produce spherical particles proved to be an inefficient technique and the particles were extremely difficult to isolate.
4. The ASTM vibratory apparatus develops an erosion intensity of 2 w/m^2. The CONCAVER system develops erosion intensities from 2,000 w/m^2 to 20,000 w/m^2. Spheroids were produced in greater quantities utilizing the ASTM vibratory apparatus than the CONCAVER system. Therefore, particle formation is not a linear function of erosion intensity.
5. All particles analyzed revealed a characteristic melted texture that accompanies the plastic flow of metals.

4.2 Recommendations

1. To expedite identification and analysis of eroded particles a system such as Chemical Particulate Pattern Recognition should be utilized. This computerized system is offered as an integral part of the scanning electron microscope analysis service utilized in this program. The system can be programmed to automatically conduct a search for predefined (in this case) spherical particles. In addition to recording dimensions, inorganic material identification, spheroid count and a plot of particle distribution, it is also possible to obtain projected area, volume, perimeter, and mass percent values.
2. A centrifuge apparatus should be utilized to separate particles from the large quantities of water obtained from the CONCAVER system.
3. Further investigations into the optimization of the parameters governing the spheroid generation tests utilizing the CONCAVER technique should be conducted. It is felt, due to the higher erosion power produced by the CONCAVER technique, that greater numbers of spherical particles should be produced than what was actually realized. Refinement of operating parameters, particle collection techniques and nozzle designs should yield larger numbers of particles.

REFERENCES

1. Hammit, F. G., "Cavitation Erosion: The State of the Art and Predicting Capability." Applied Mechanics Review. Volume 32, No. 6. June 1979.

2. Thiruvengadam, A. P., "Spheroids Produced by Cavitation Erosion." Naval Research Reviews. May 1978.

3. Thiruvengadam, A. P., "Mechanism of Formation of Spheroids Produced by Cavitation Erosion." Presentation at the 32nd annual meeting of the American Engineers. December 1976.

4. Plesset, M. S. and R. B. Chapman, "Collapse of an Initially Spherical Vapor Cavity in the Neighborhood of a Solid Boundary." Rep. 85-49. California Institute of Technology, Division of Engineering. June 1970

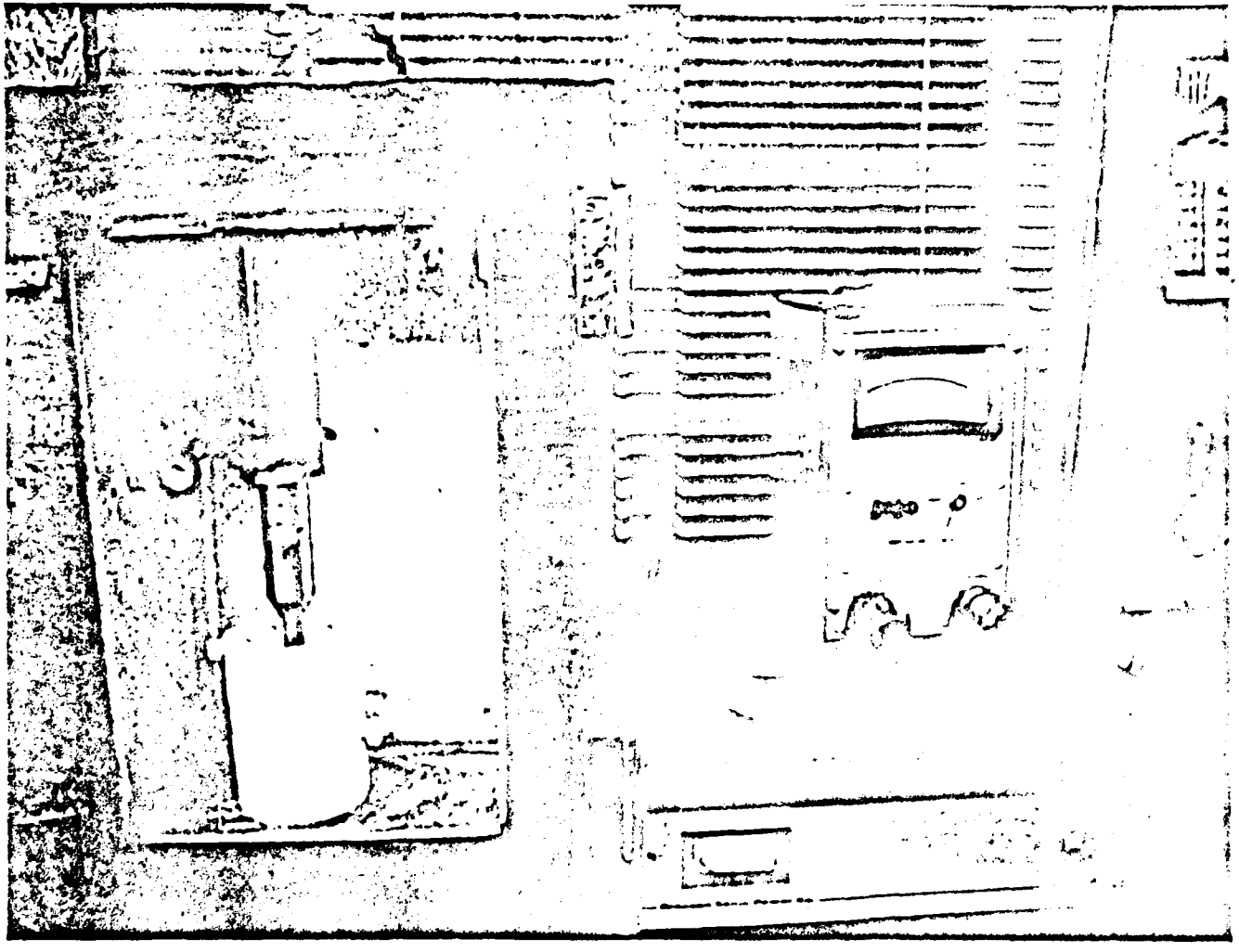

THIS PAGE IS BEST QUALITY PRACTICABLE
FROM COPY FURNISHED TO DDC

FIGURE 1 ASTM STANDARD VIBRATORY APPARATUS

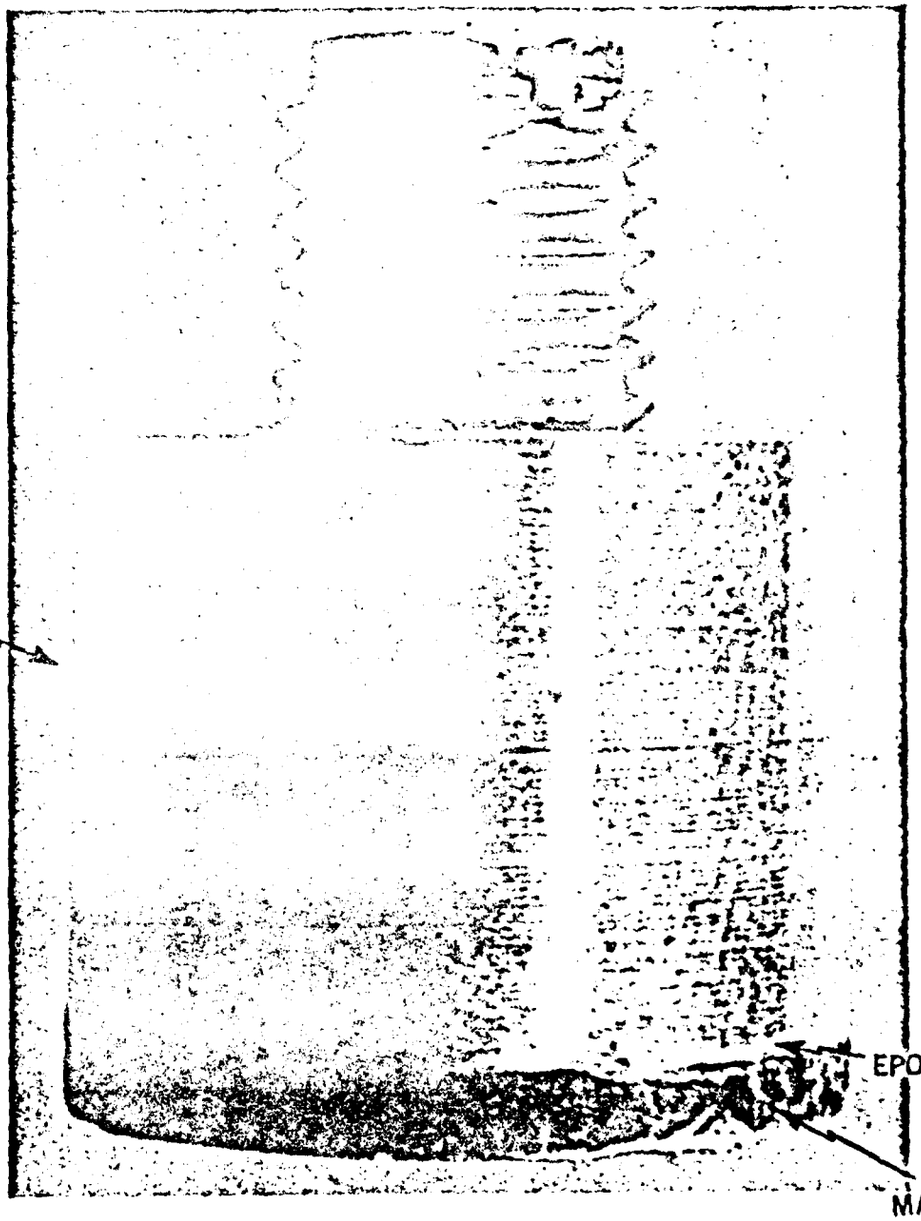

FIGURE 2 MODIFIED ALUMINUM BUTTON WITH LEAD PLATE ATTACHED

THIS PAGE IS BEST QUALITY PRACTICABLE
FROM COPY FURNISHED TO DDC

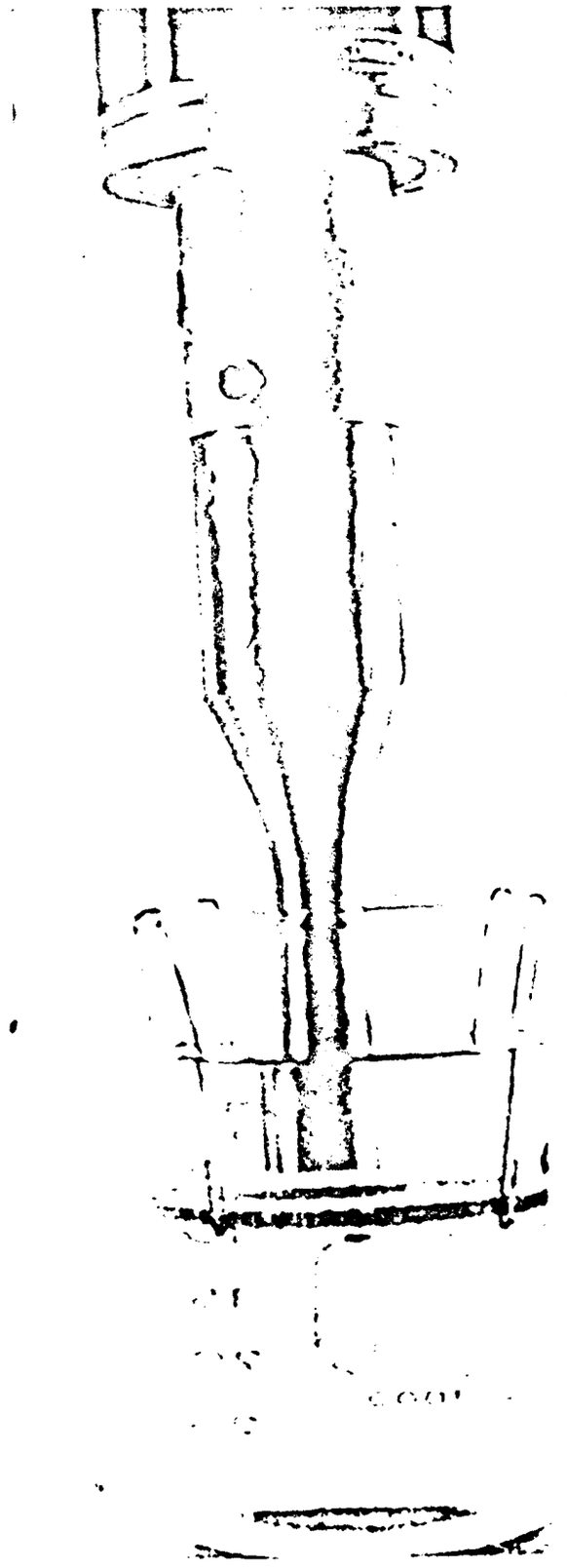

THIS PAGE IS BEST QUALITY PRACTICABLE
FROM COPY FURNISHED TO DDC

FIGURE 3 VIBRATORY TEST APPARATUS USED TO ERODE
1/8 INCH LEAD SPECIMEN PLATE

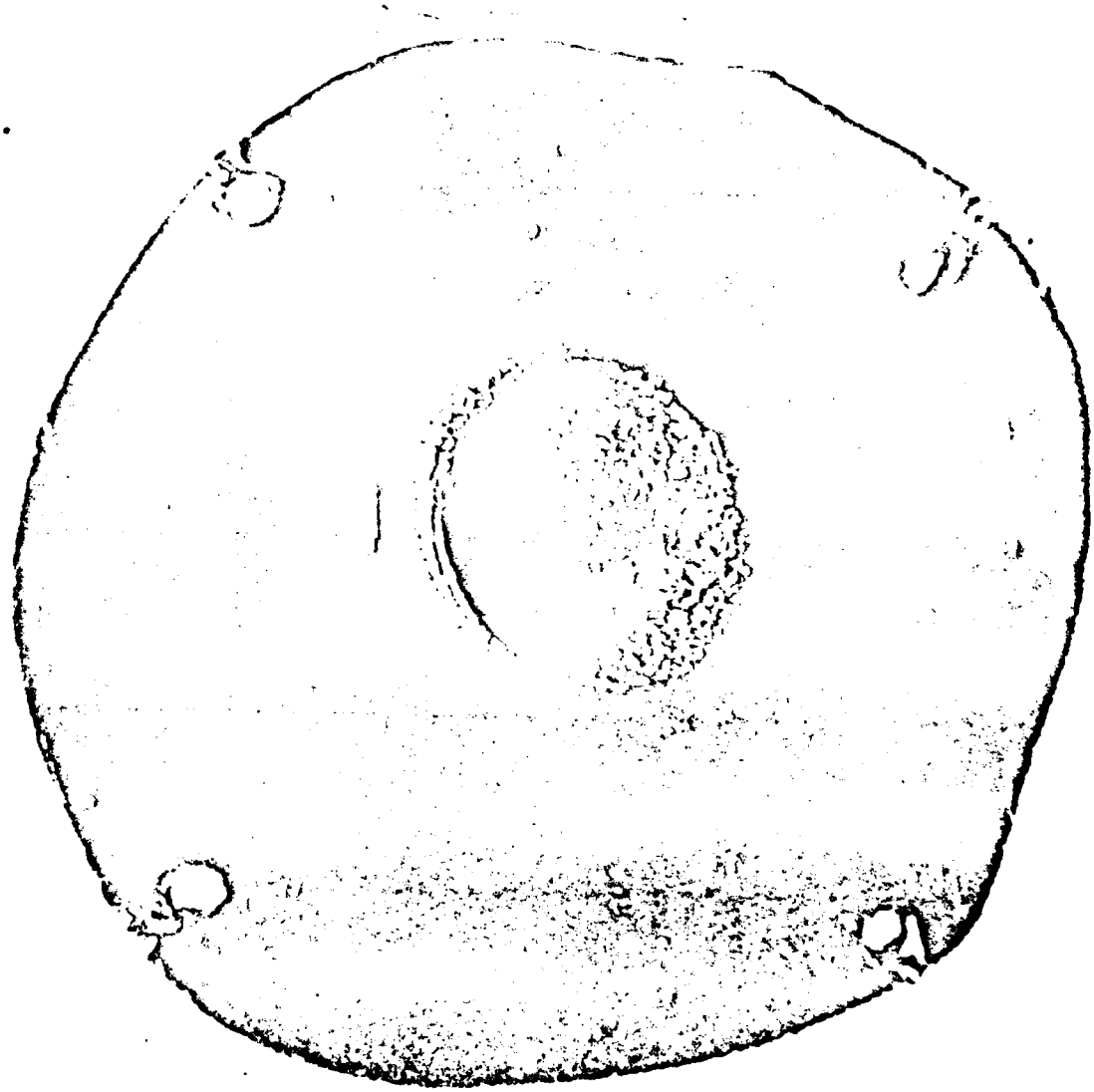

FIGURE 4 LEAD SPECIMEN THAT WAS ERODED IN DISTILLED WATER BY TITANIUM BUTTON

THIS PAGE IS BEST QUALITY PRACTICABLE
FROM COPY FURNISHED TO DDC

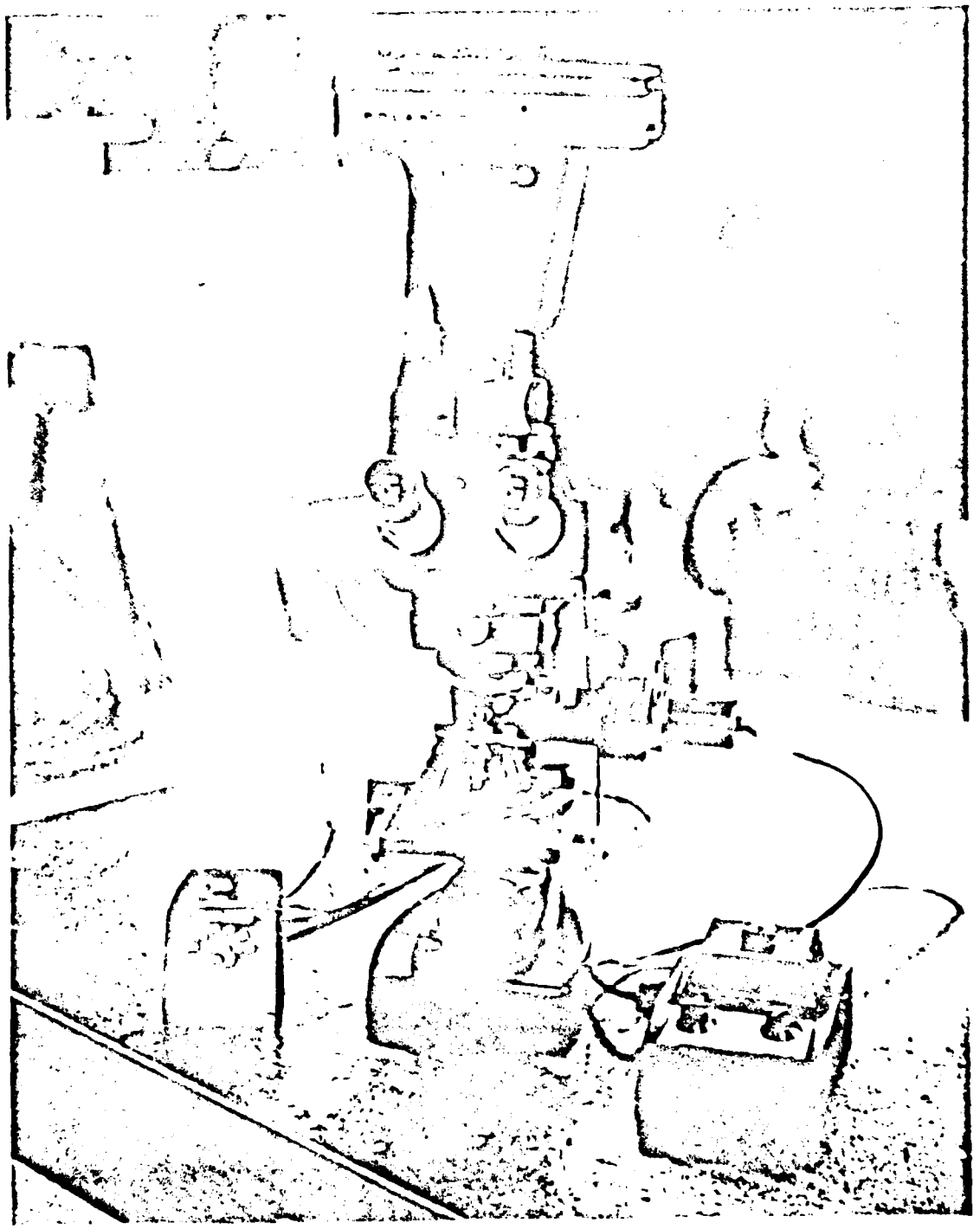

FIGURE 5 METALLURGICAL MICROSCOPE USED TO MEASURE PARTICLE DIAMETERS

THIS PAGE IS BEST QUALITY PRACTICABLE
FROM COPY FURNISHED TO DDC

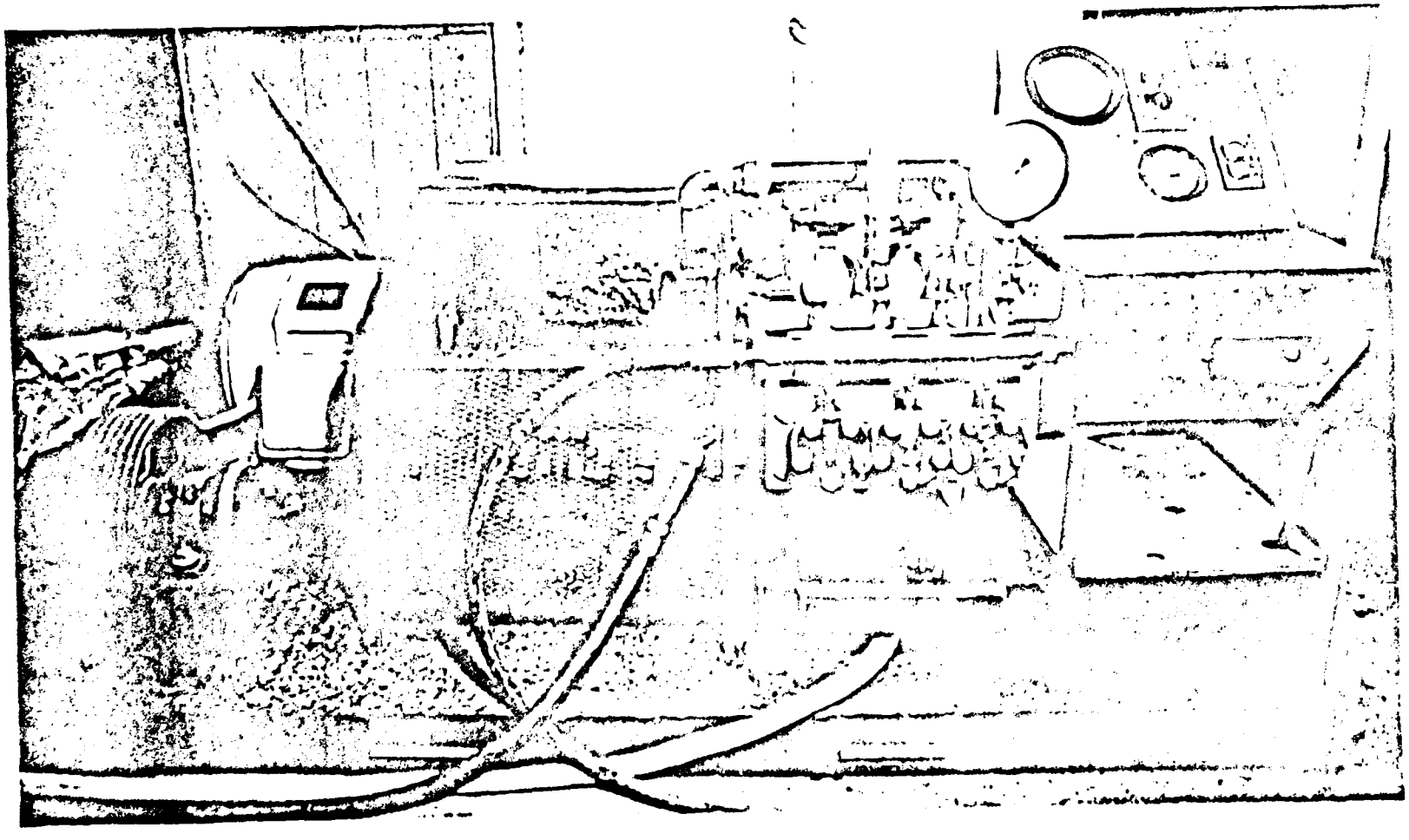

THIS PAGE IS BEST QUALITY PRACTICABLE
FROM COPY FURNISHED TO DDC

FIGURE 6 TRIPLEX PLUNGER PUMP AND MOTOR COMBINATION CAPABLE OF 5 GPM AT 20.000 PSI

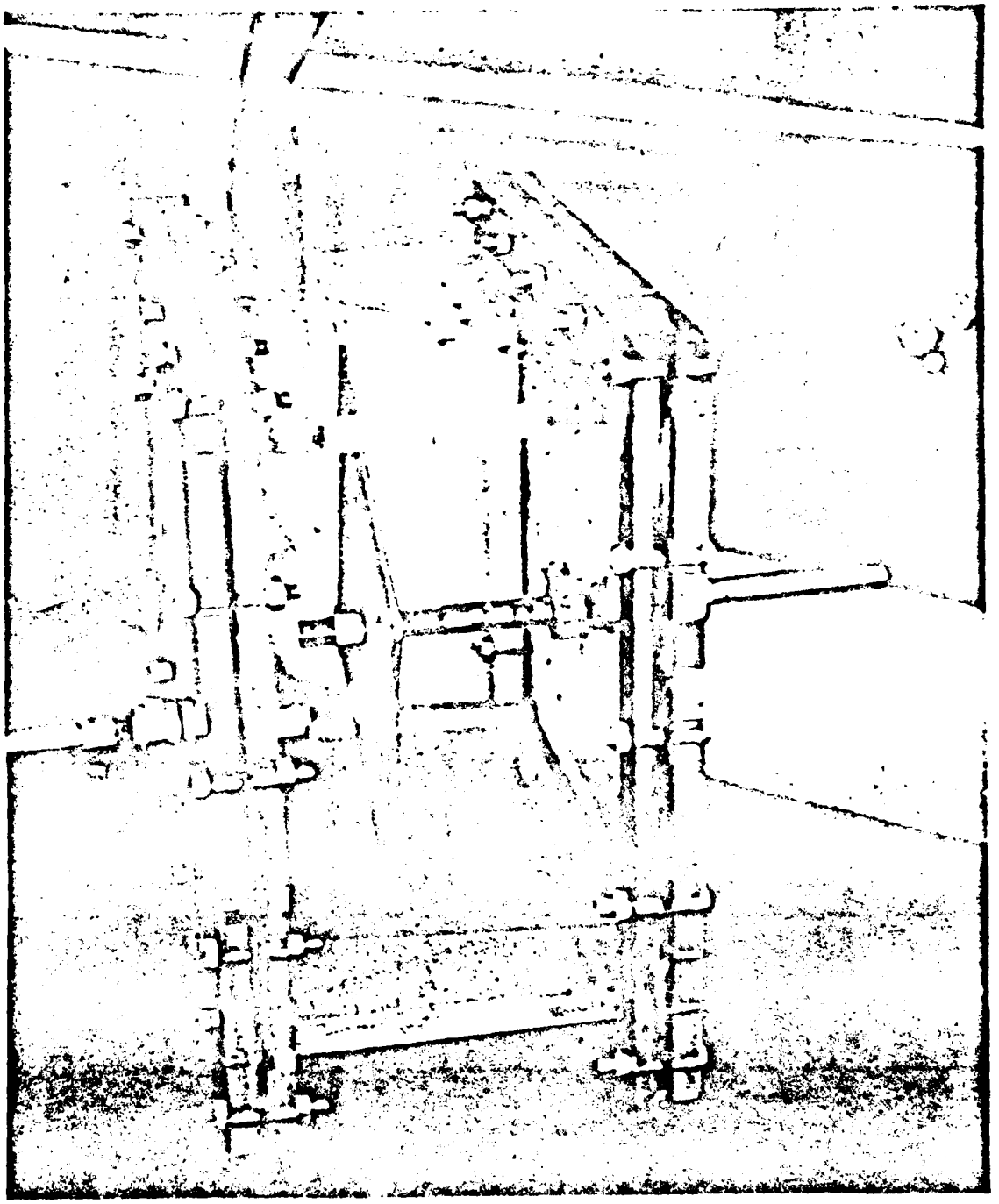

FIGURE 7 PARTICLE COLLECTION CHAMBER

THIS PAGE IS BEST QUALITY PRACTICABLE
FROM COPY FURNISHED TO DDC

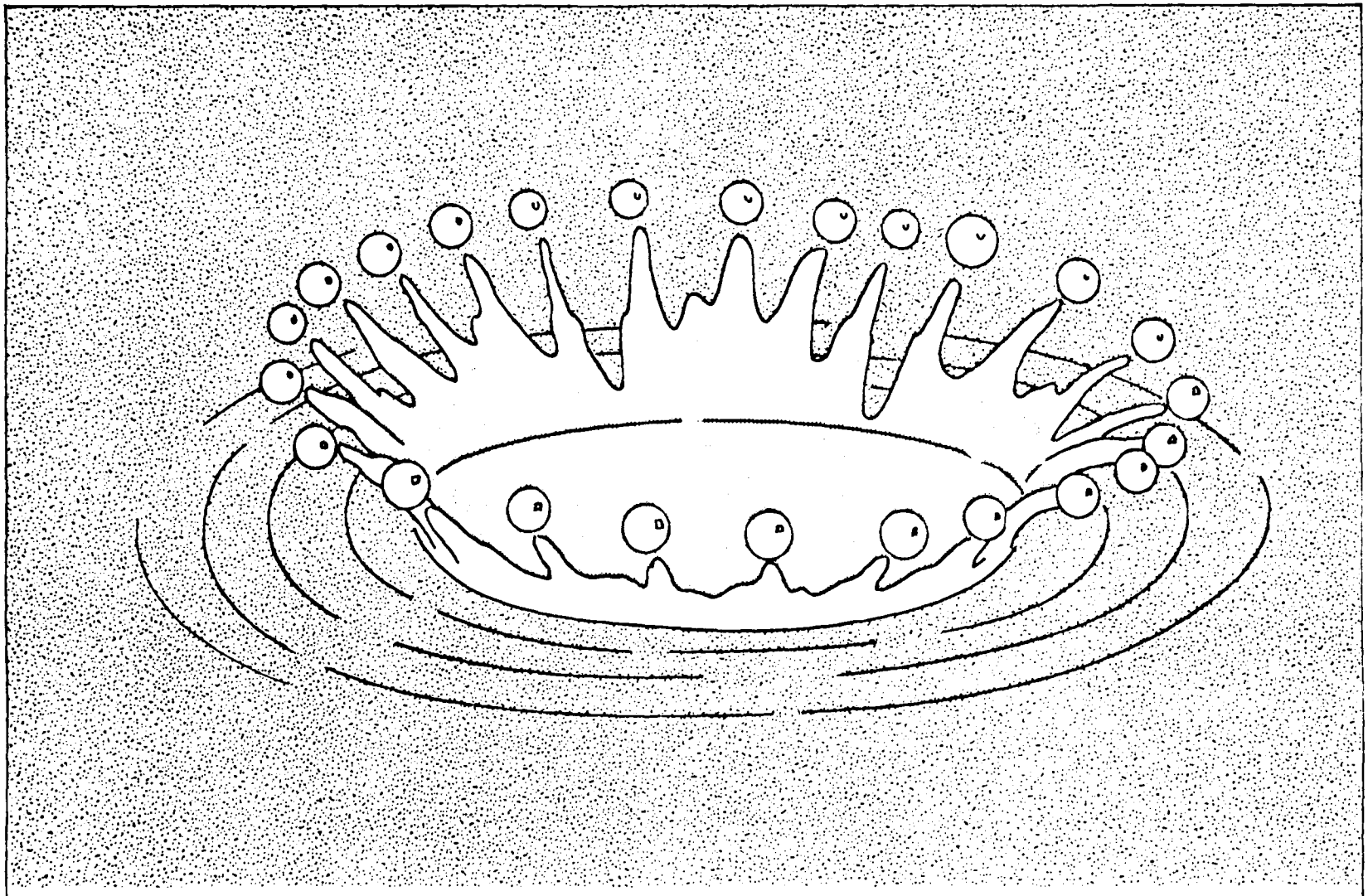

FIGURE 8 SKETCH OF EDGERTON'S HIGH SPEED PHOTOGRAPH OF A MILKDROP ILLUSTRATING THE SPLASH-SPRAY THEORETICAL RESULT

THIS PAGE IS BEST QUALITY PRACTICABLE
FROM COPY FURNISHED TO DDC

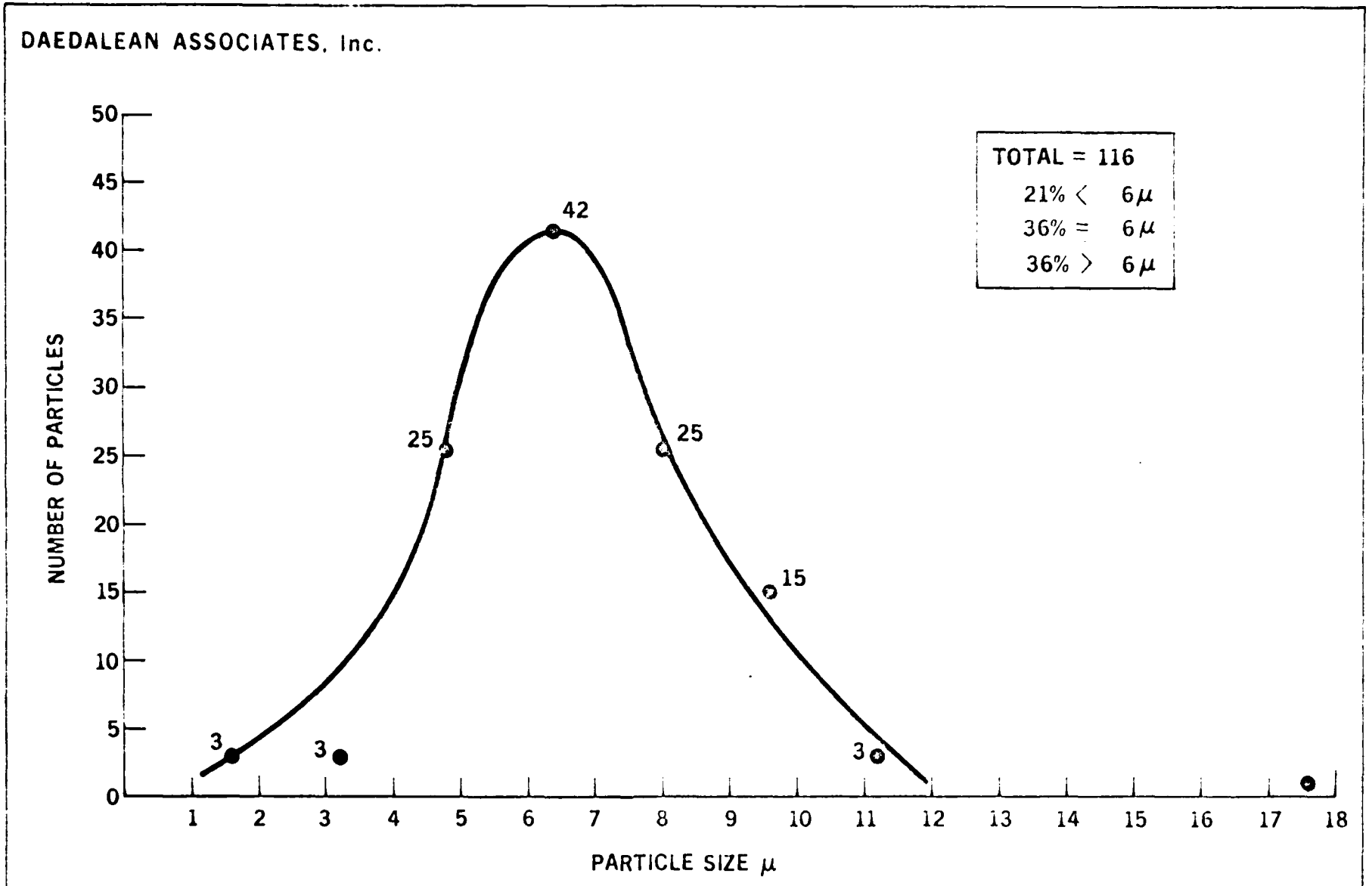

FIGURE 9 PARTICLE SIZE DISTRIBUTION CURVE FOR MONEL SPHERICAL PARTICLES GENERATED FROM EROSION IN DISTILLED WATER

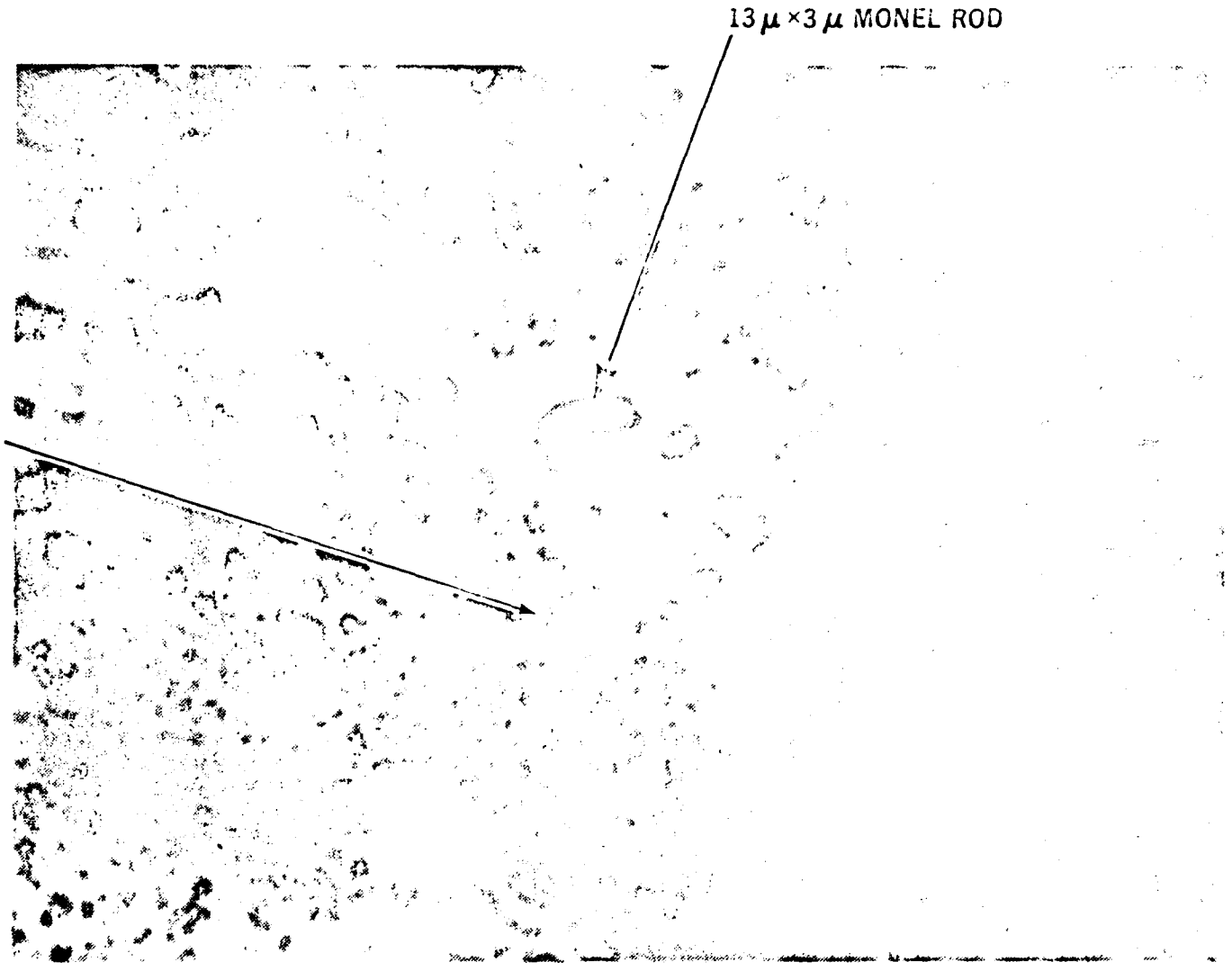

THIS PAGE IS BEST QUALITY PRACTICABLE
FROM COPY FURNISHED TO DDC

FIGURE 10 PHOTOMICROGRAPH OF A 13μ LONG 3μ WIDE MONEL ROD WITH TWO 6μ SPHERICAL PARTICLES LOCATED DIRECTLY BELOW

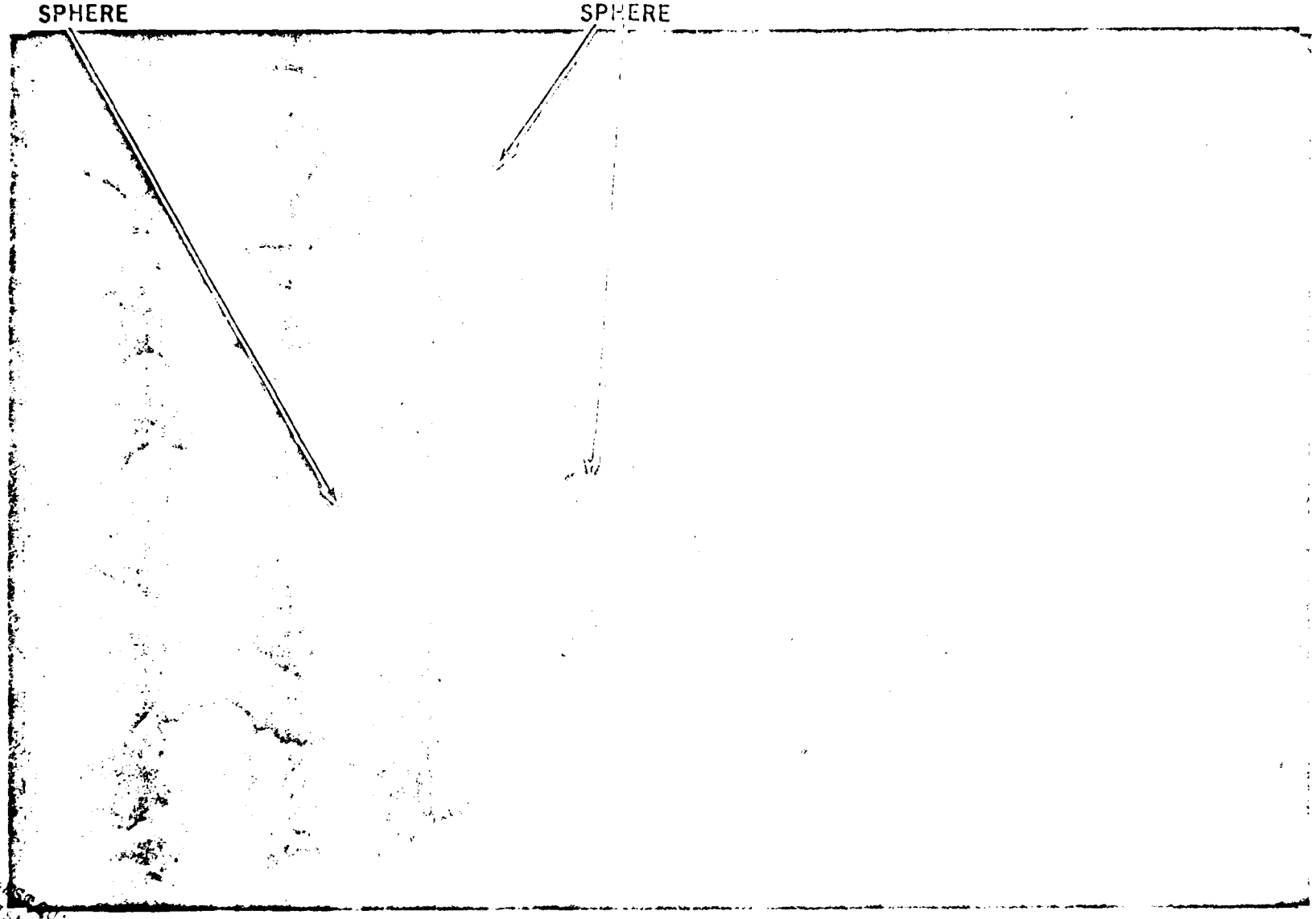

FIGURE 11 SCANNING ELECTRON PHOTOMICROGRAPH OF MONEL PARTICLES GENERATED FROM EROSION IN DISTILLED WATER

THIS PAGE IS BEST QUALITY PRACTICABLE
FROM COPY FURNISHED TO DDC

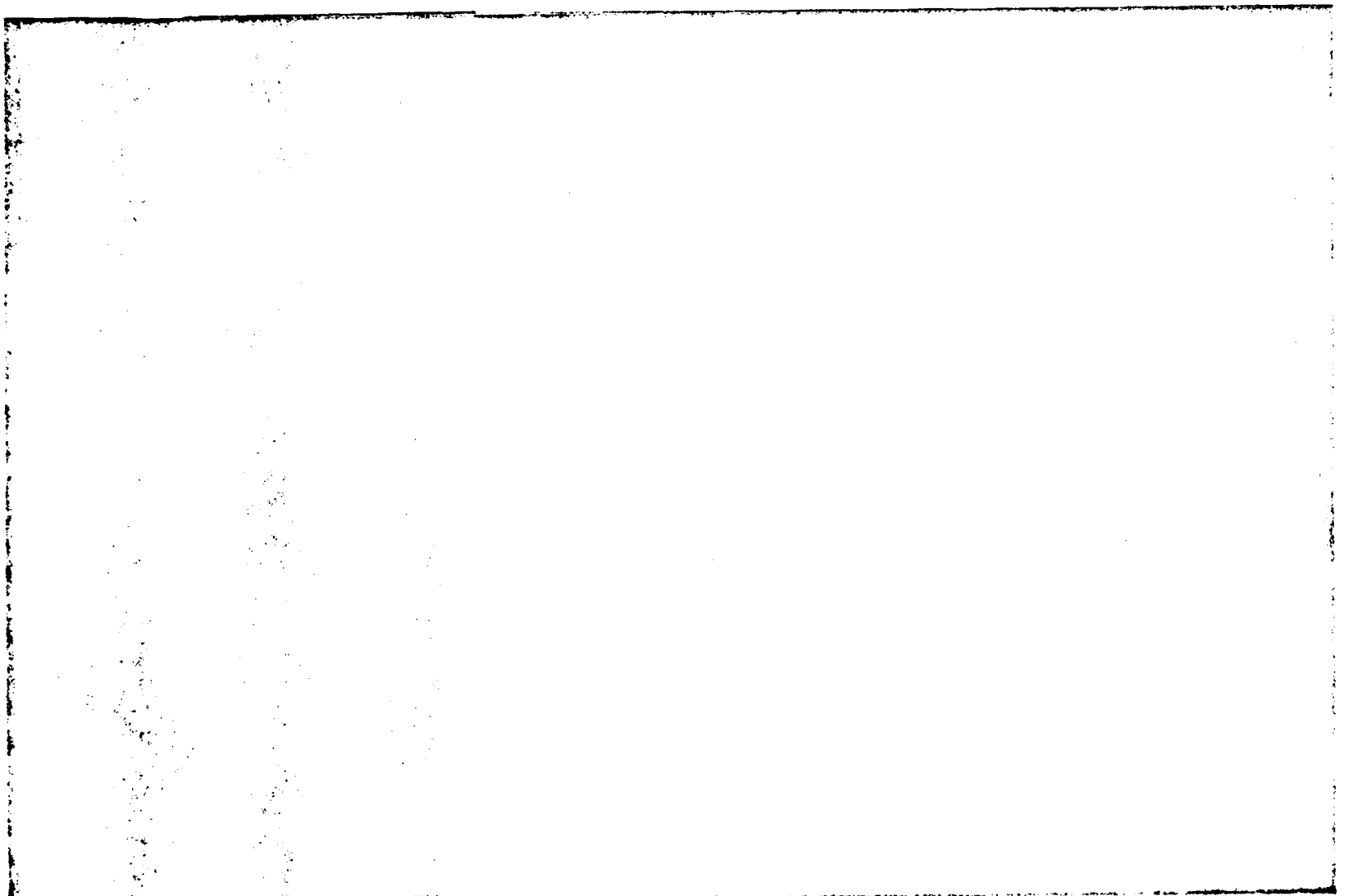

FIGURE 12 SCANNING ELECTRON PHOTOMICROGRAPH OF TWO MONEL SPHERICAL PARTICLES GENERATED FROM EROSION IN DISTILLED WATER

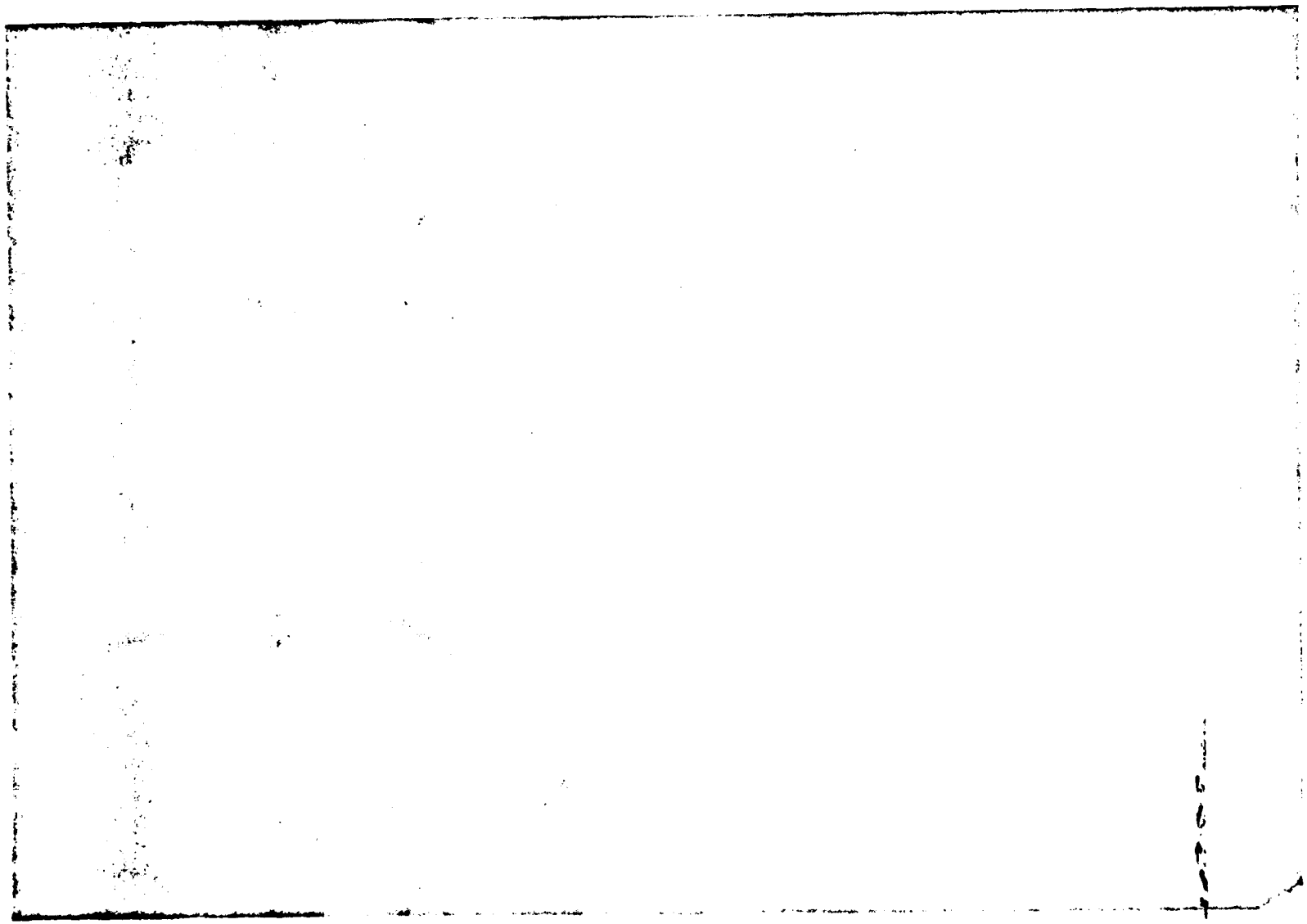

THIS PAGE IS BEST QUALITY PRACTICABLE
FROM COPY FURNISHED TO DDC

FIGURE 13 SCANNING ELECTRON PHOTOMICROGRAPH OF AN 11μ MONEL SPHERICAL PARTICLE GENERATED FROM EROSION IN DISTILLED WATER

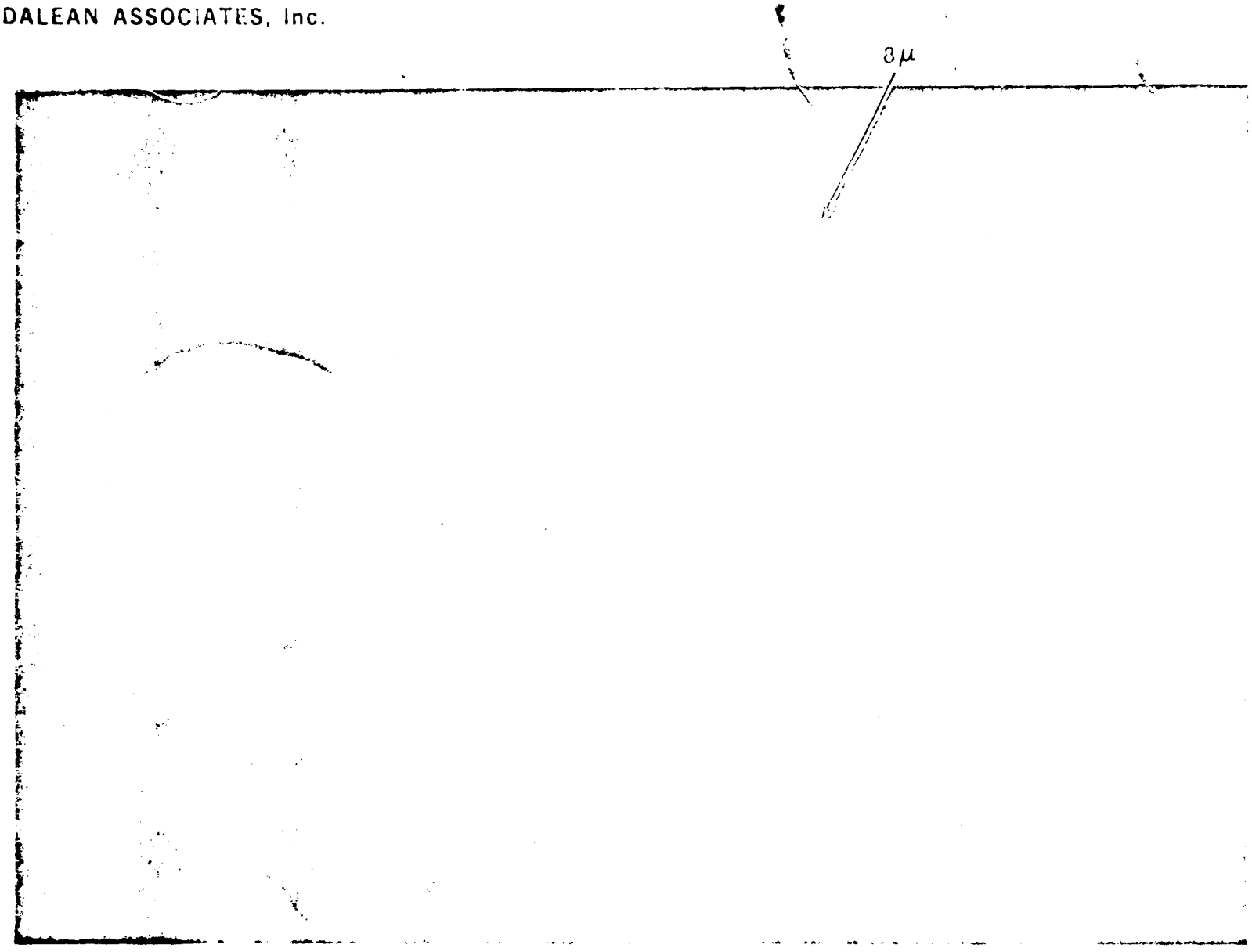

FIGURE 14 SCANNING ELECTRON PHOTOMICROGRAPH OF AN 8μ MONEL SPHERICAL PARTICLE GENERATED FROM EROSION IN DISTILLED WATER

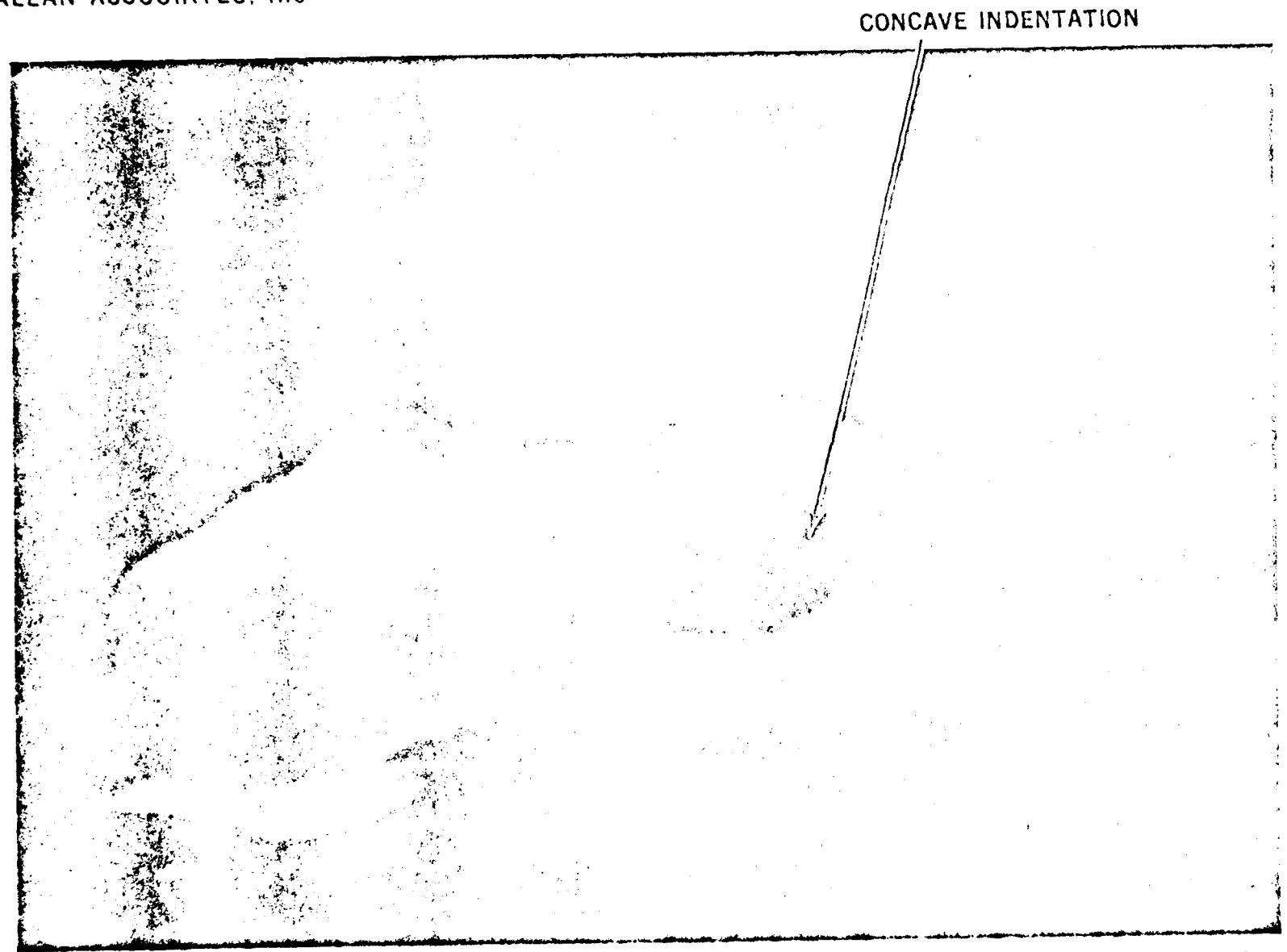

FIGURE 15 SCANNING ELECTRON PHOTOMICROGRAPH OF A 6μ MONEL SPHERICAL PARTICLE GENERATED FROM EROSION IN DISTILLED WATER, SHOWING CRATERLIKE INDENTATION

THIS PAGE IS BEST QUALITY PRACTICABLE
FROM COPY FURNISHED TO DDC

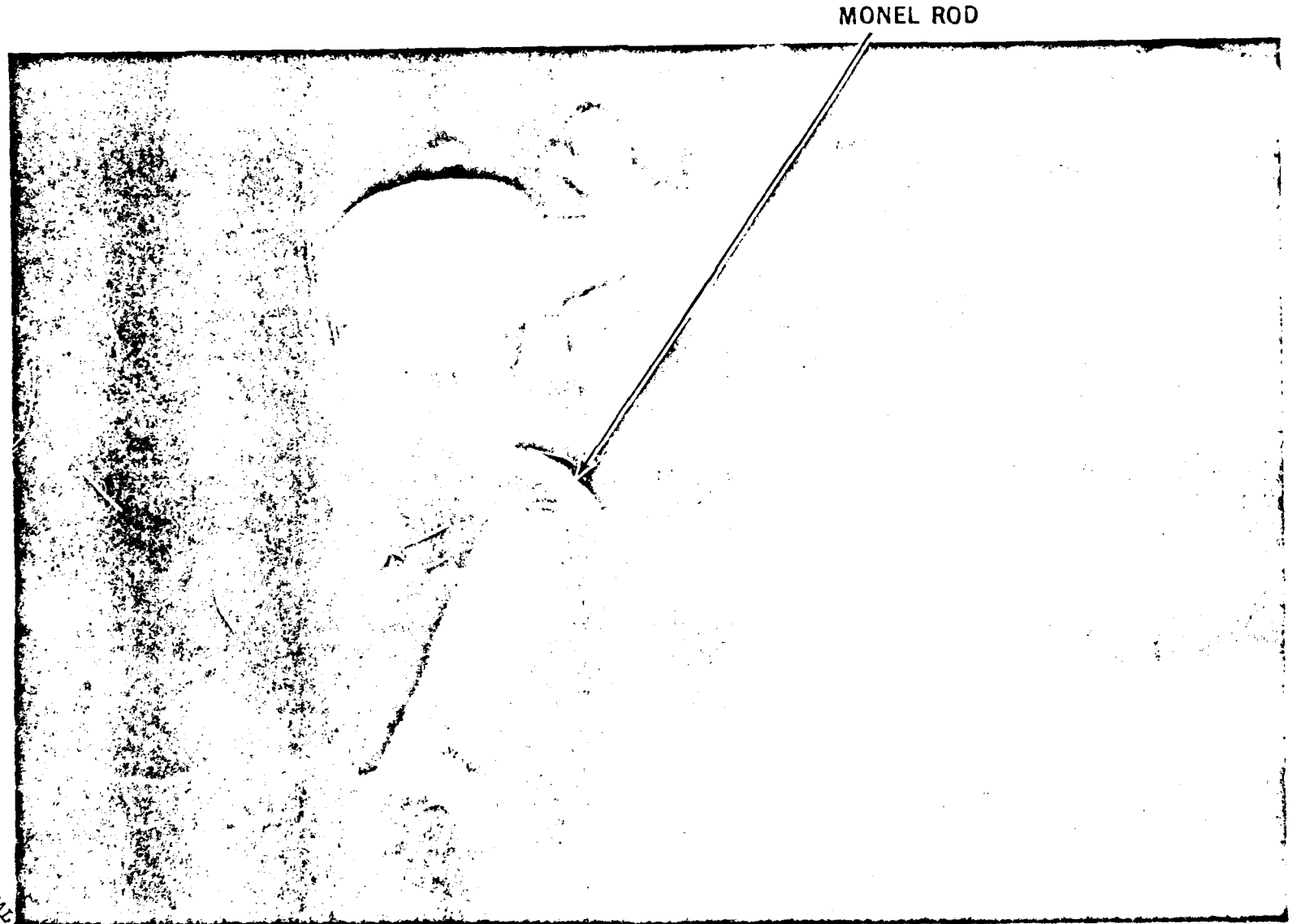

FIGURE 16 SCANNING ELECTRON PHOTOMICROGRAPH OF A 12 μ LONG, 4 μ DIAMETER CYLINDRICAL MONEL ROD GENERATED FROM EROSION IN DISTILLED WATER

THIS PAGE IS BEST QUALITY PRACTICABLE
FROM COPY FURNISHED TO DDC

DAEDALEAN ASSOCIATES, Inc.

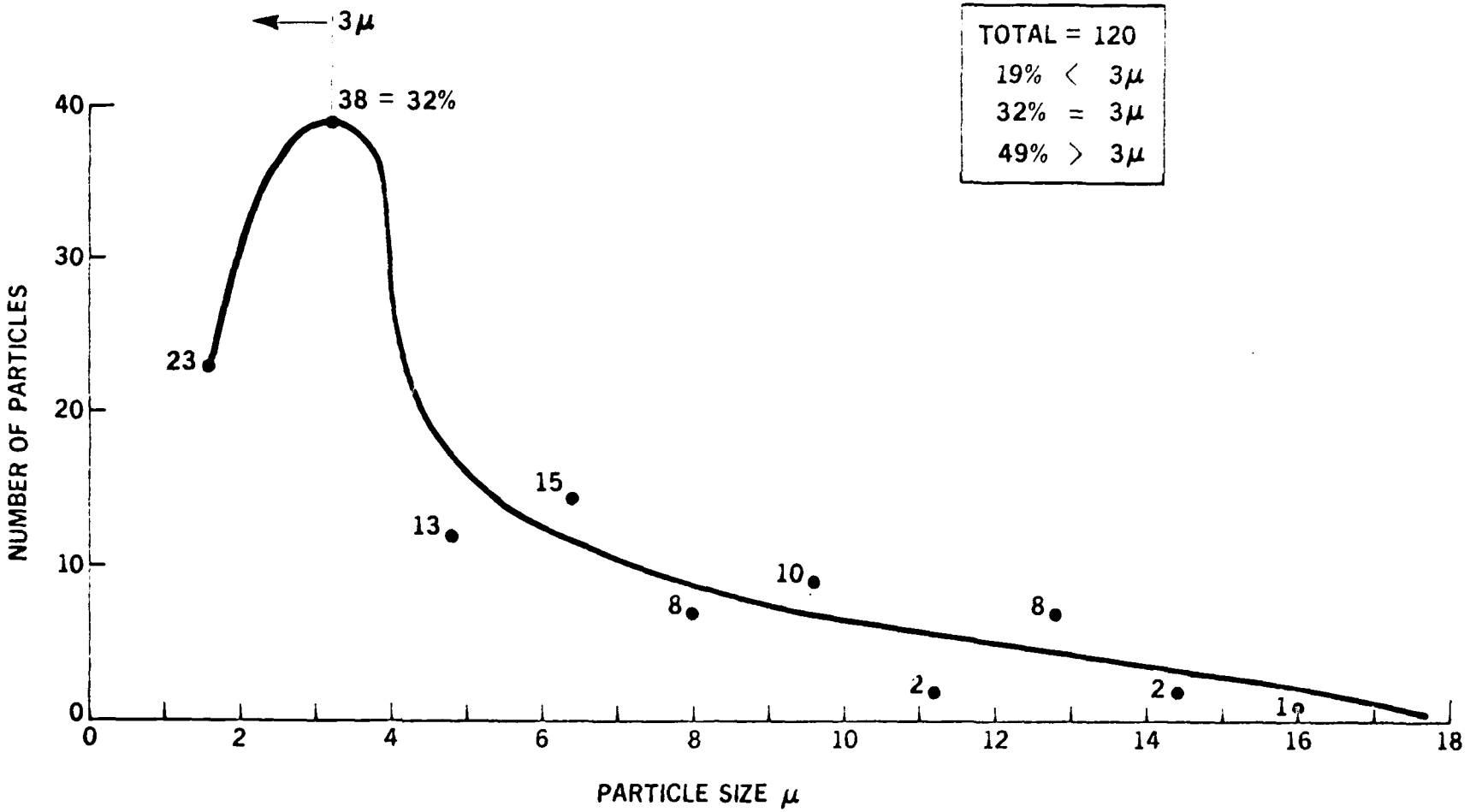

FIGURE 17 PARTICLE SIZE DISTRIBUTION CURVE FOR MONEL SPHERICAL PARTICLES GENERATED FROM EROSION IN 10W OIL

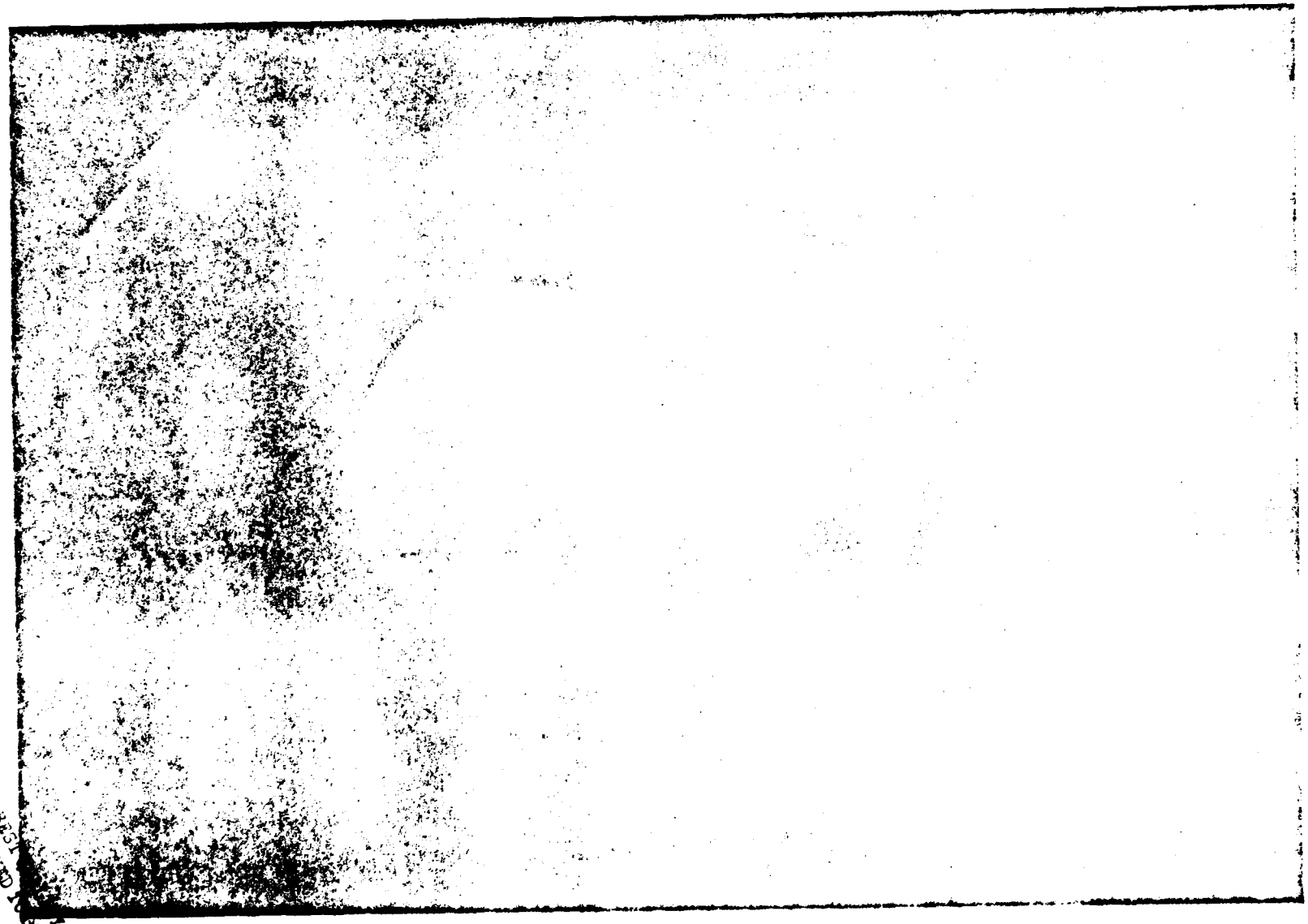

FIGURE 18 SCANNING ELECTRON PHOTOMICROGRAPH OF A 10μ MONEL SPHERICAL PARTICLE GENERATED FROM EROSION IN 10W OIL

THIS PAGE IS BEST QUALITY PRACTICABLE
FROM COPY FURNISHED TO DDC

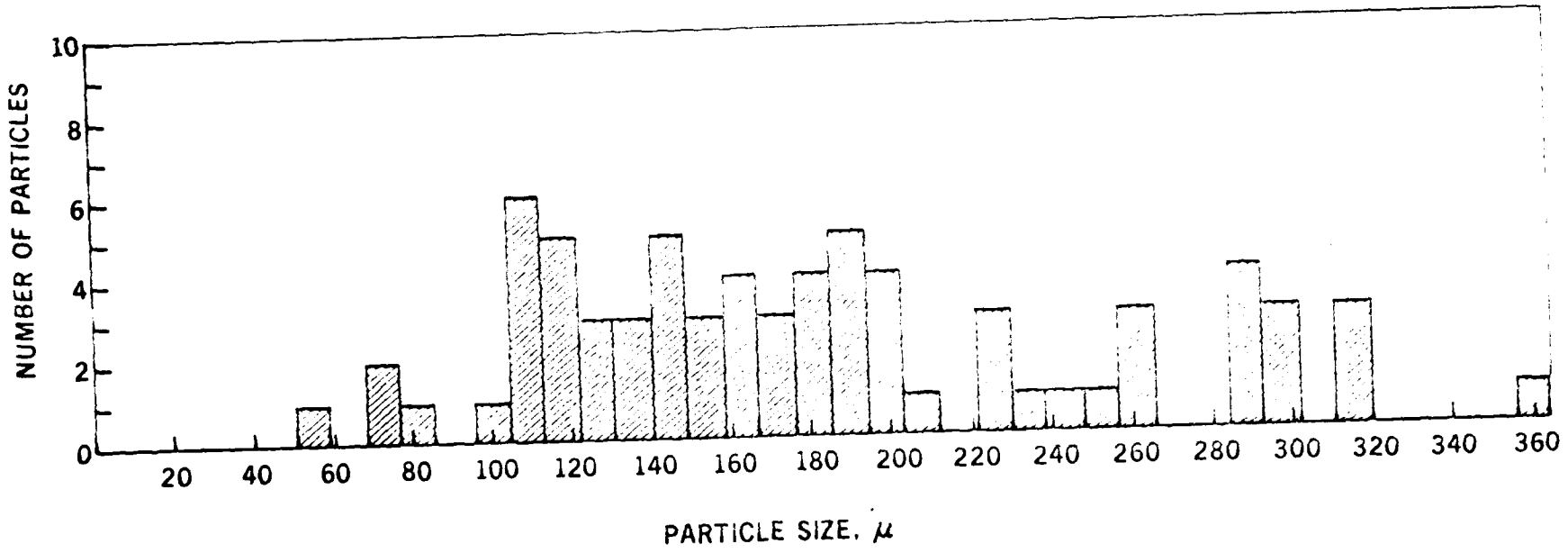

FIGURE 19 PARTICLE SIZE HISTOGRAM FOR LEAD SPHERICAL PARTICLES GENERATED FROM EROSION IN DISTILLED WATER

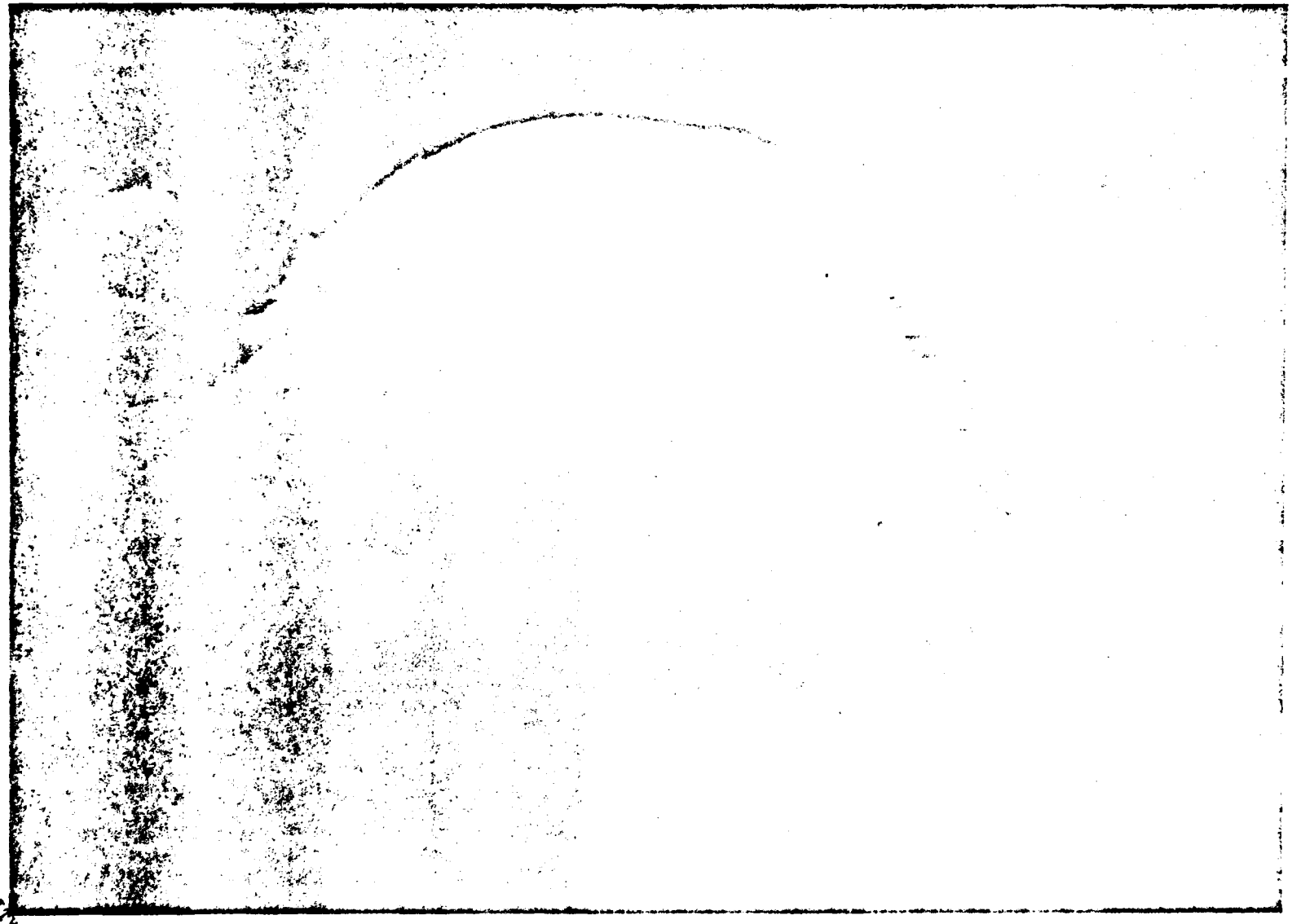

FIGURE 20 SCANNING ELECTRON PHOTOMICROGRAPH OF A 40 μ LEAD SPHEROID GENERATED FROM EROSION IN DISTILLED WATER

THIS PAGE IS BEST QUALITY PRACTICABLE
FROM COPY FURNISHED TO DDC

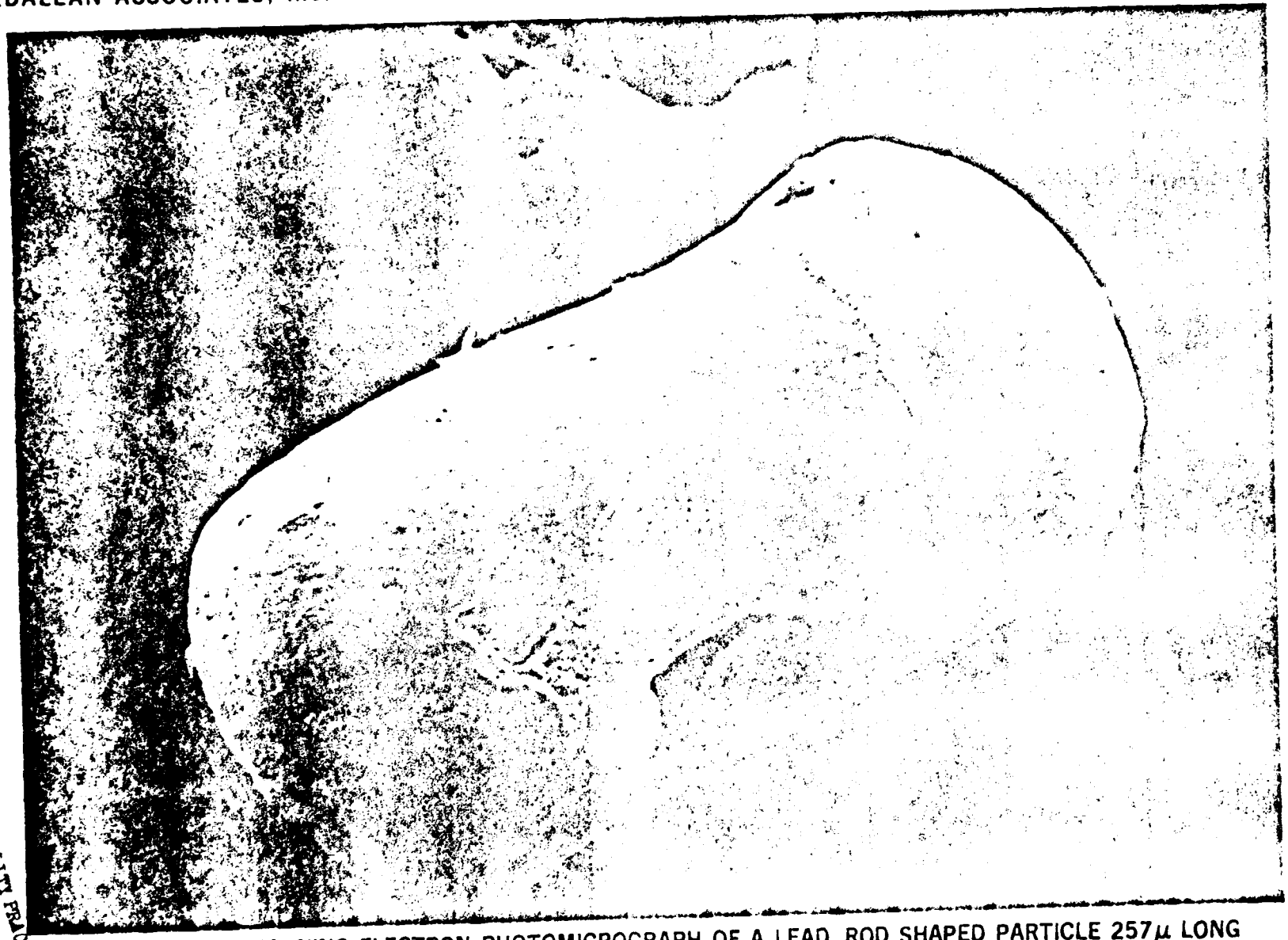

FIGURE 21 SCANNING ELECTRON PHOTOMICROGRAPH OF A LEAD, ROD SHAPED PARTICLE 257μ LONG AND 123μ IN DIAMETER GENERATED FROM EROSION IN DISTILLED WATER

THIS PAGE IS BEST QUALITY PRACTICABLE
FROM COPY FURNISHED TO DTIC

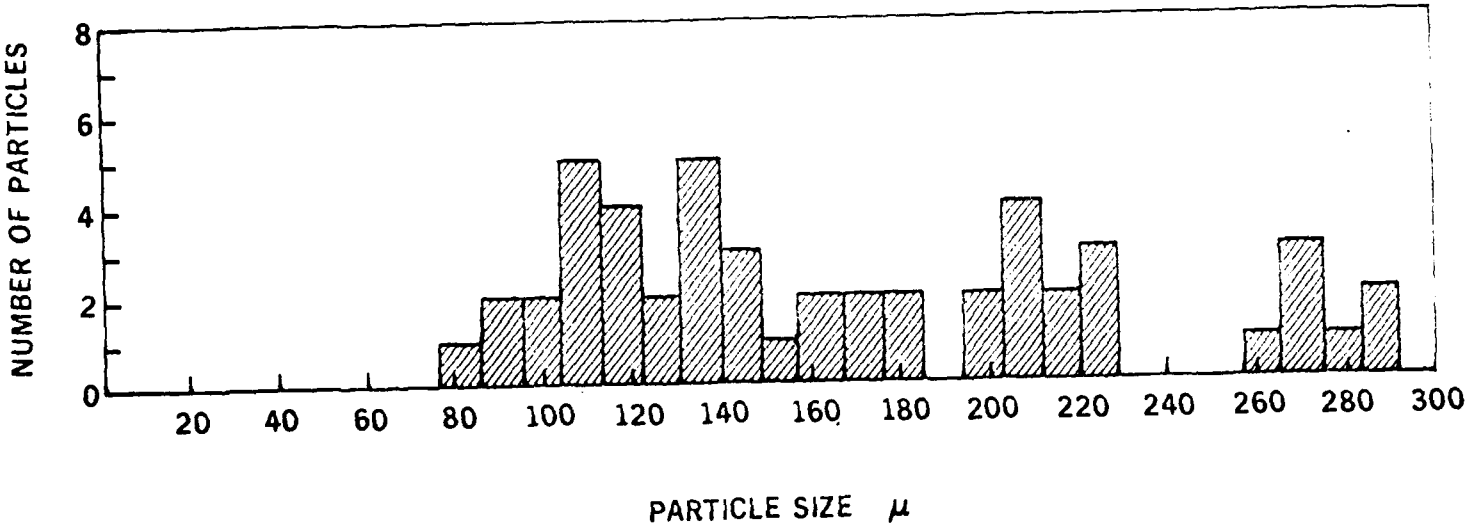

FIGURE 22 PARTICLE SIZE HISTOGRAM FOR LEAD SPHERICAL PARTICLES GENERATED FROM EROSION IN 10W OIL

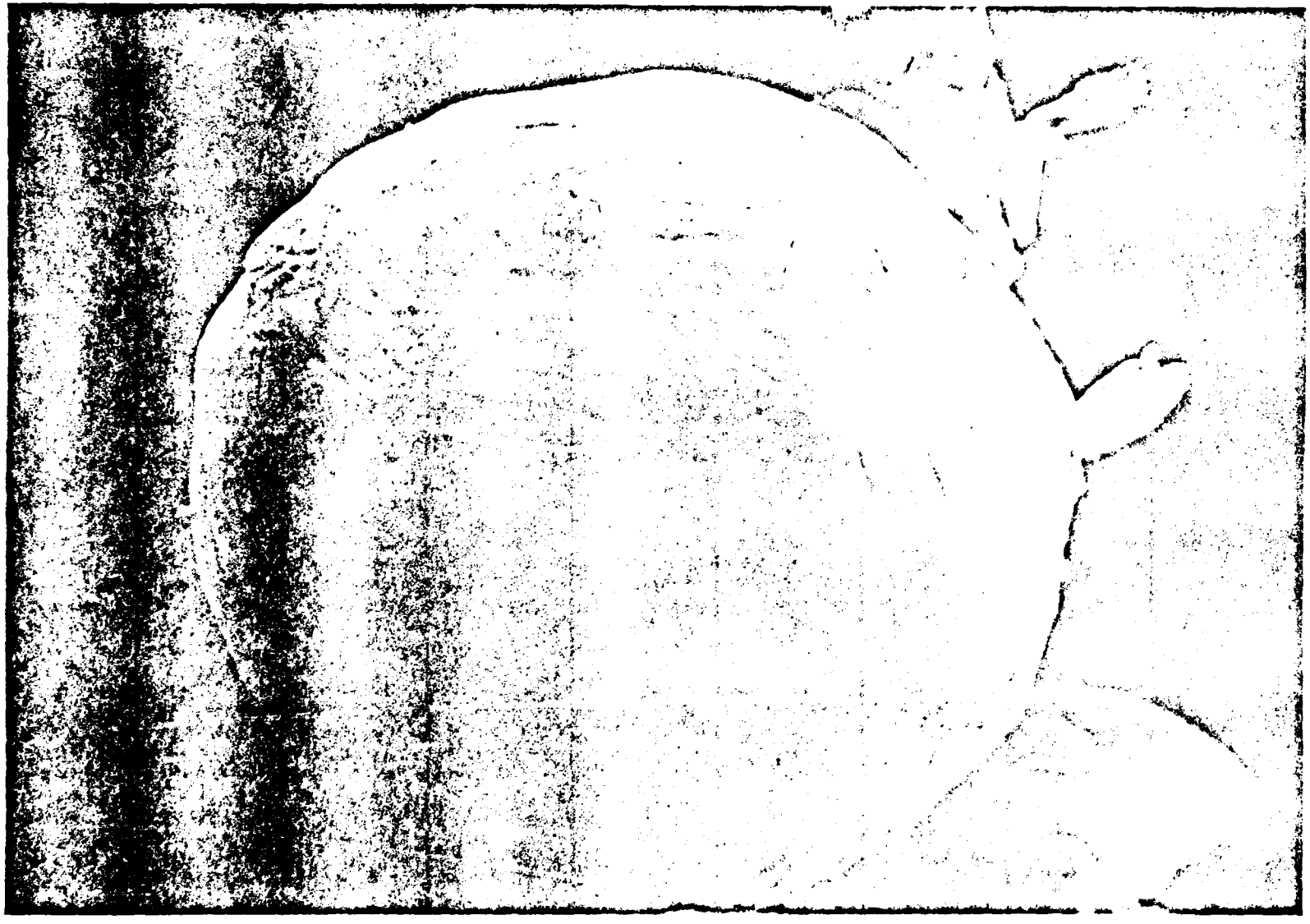

FIGURE 23 SCANNING ELECTRON PHOTOMICROGRAPH OF A 390μ LEAD SPHEROID, REVEALING SURFACE ABRASIONS, GENERATED FROM EROSION IN 10W OIL

THIS PAGE IS BEST QUALITY PRACTICABLE
FROM COPY FURNISHED TO DDC

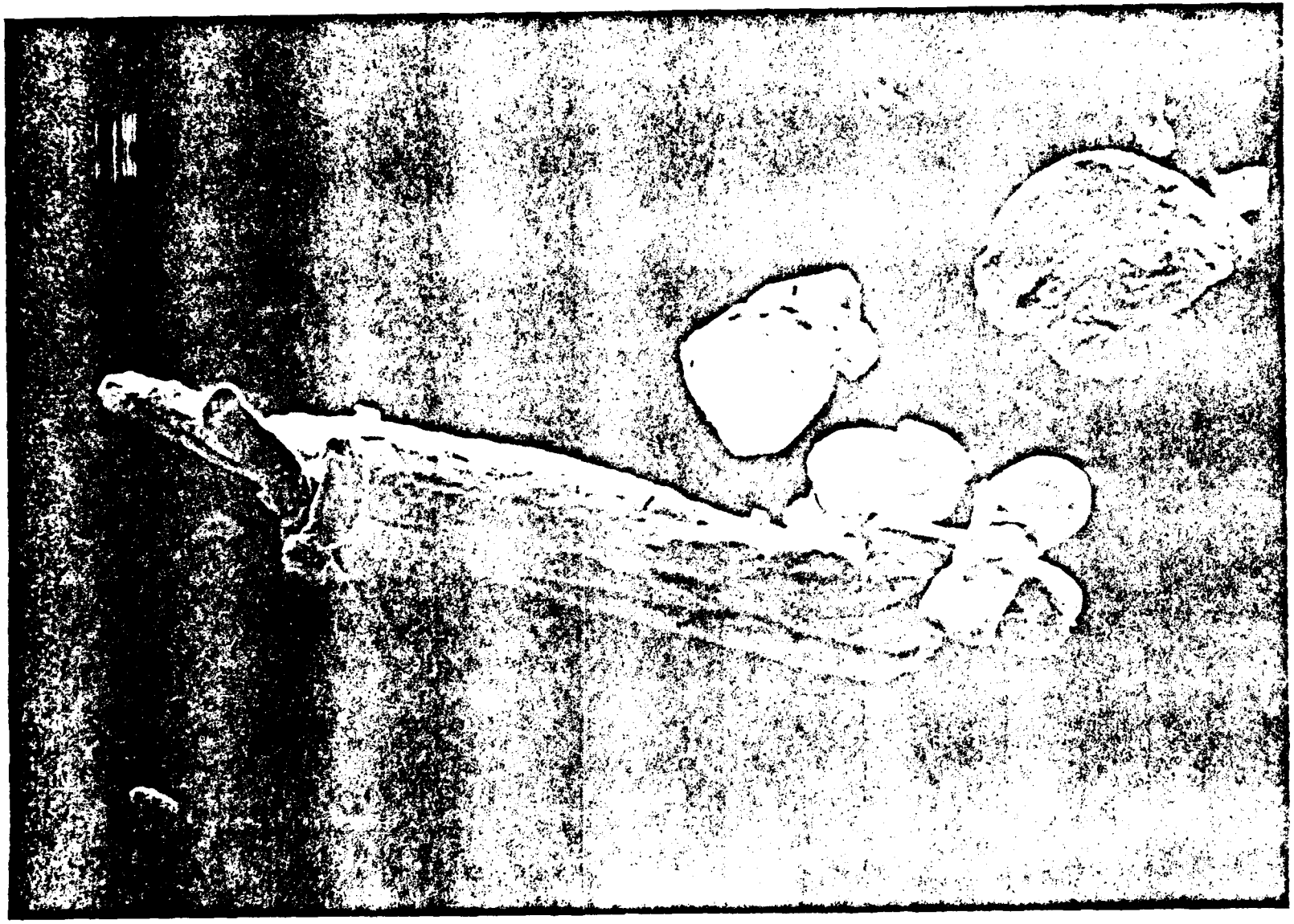

FIGURE 24 SCANNING ELECTRON PHOTOMICROGRAPH OF A ROD SHAPED, LEAD PARTICLE 375μ LONG AND 70μ IN DIAMETER

THIS PAGE IS BEST QUALITY PRACTICABLE
FROM COPY FURNISHED TO DDC

35μ LEAD SPHEROID

THIS PAGE IS
FROM COPY FU
TO DDC
IT FRACTICABLE

FIGURE 25 SCANNING ELECTRON PHOTOMICROGRAPH OF A 35μ LEAD SPHEROID SOLIDIFIED DURING FORMATION

DAEDALEAN ASSOCIATES, Inc.

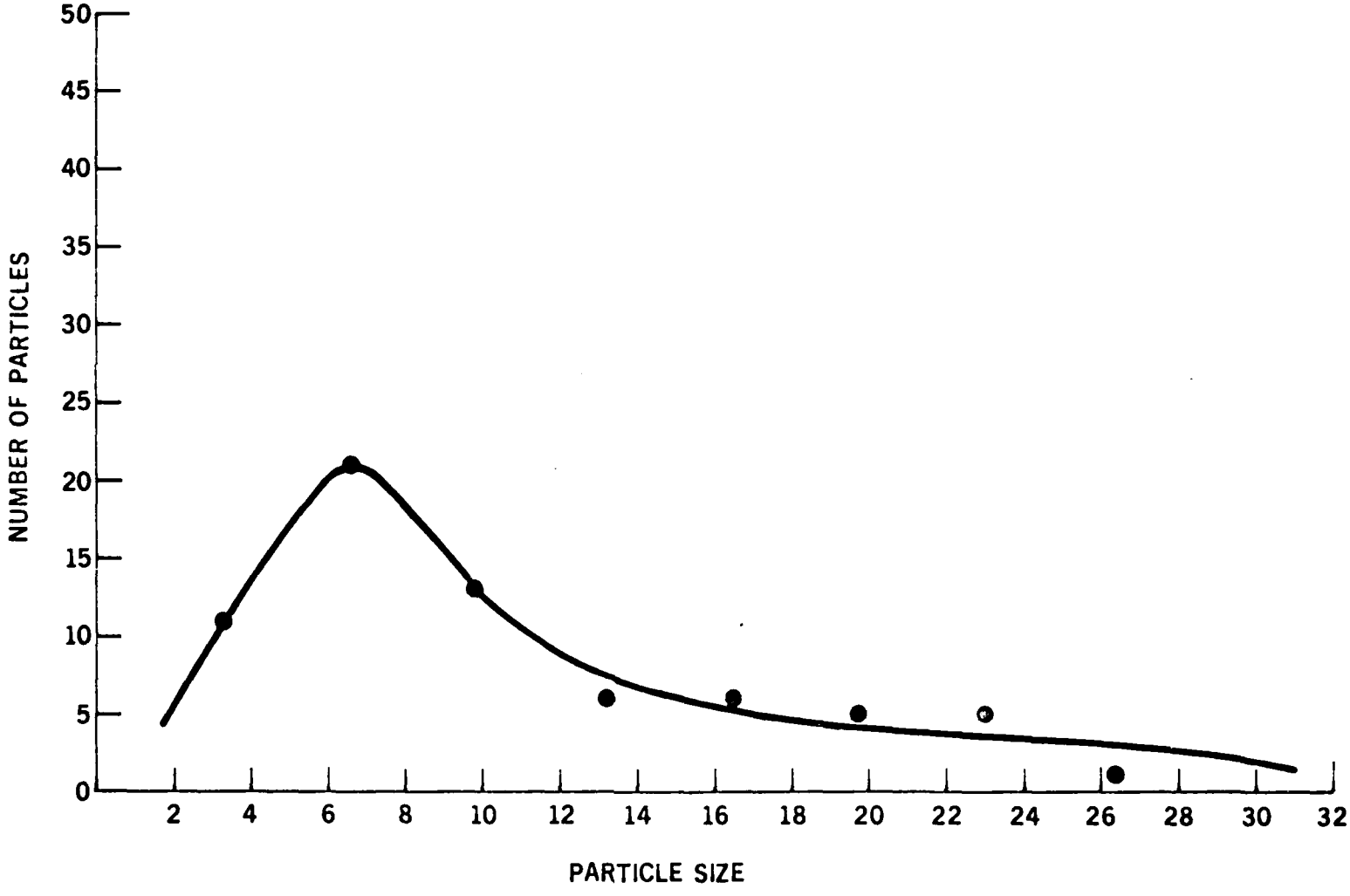

FIGURE 26 PARTICLE SIZE DISTRIBUTION CURVE FOR ALUMINUM SPHERICAL PARTICLES GENERATED FROM EROSION IN 10W OIL

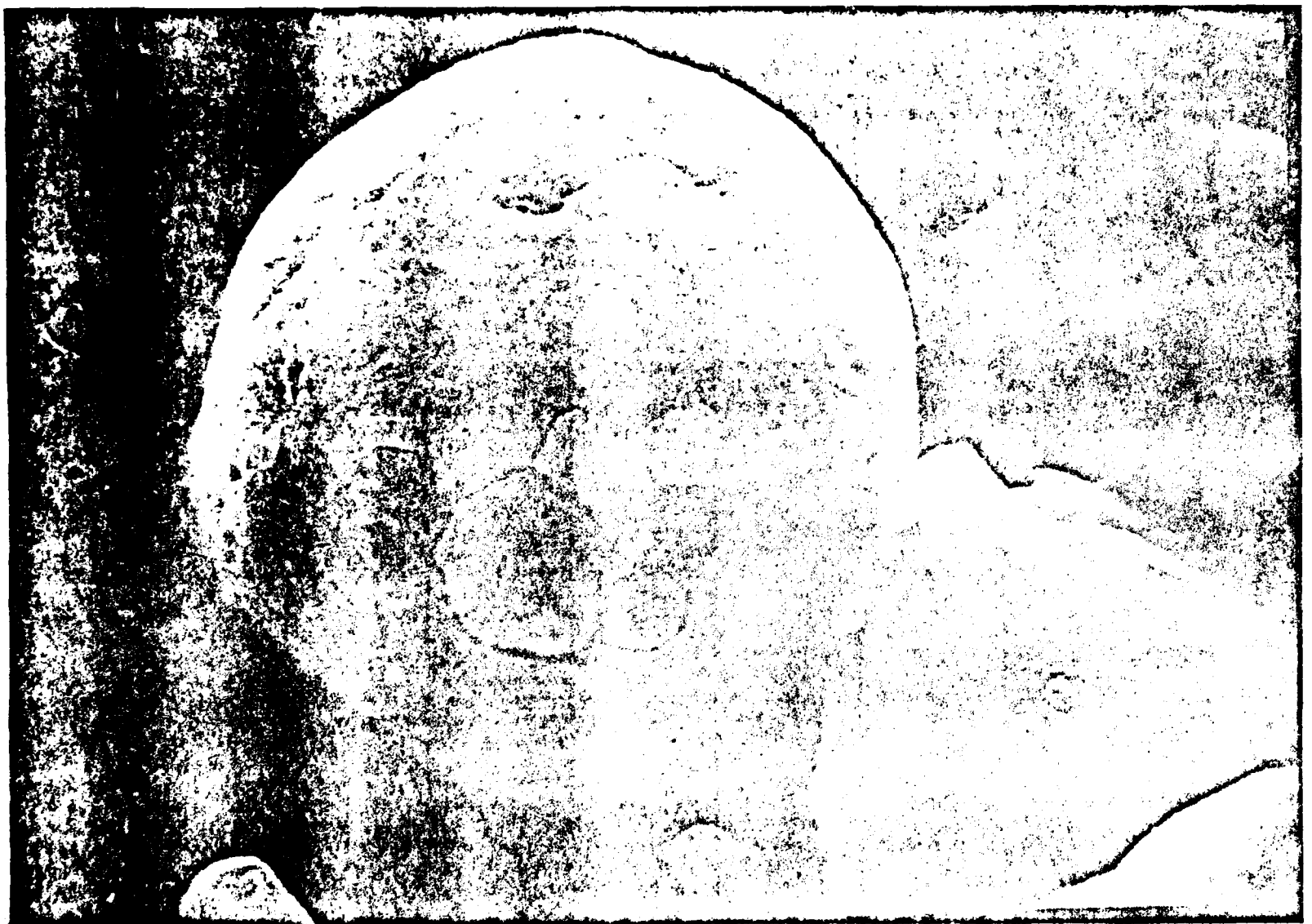

FIGURE 27 SCANNING ELECTRON PHOTOMICROGRAPH OF A 65μ ALUMINUM SPHEROID GENERATED FROM EROSION IN 10W OIL

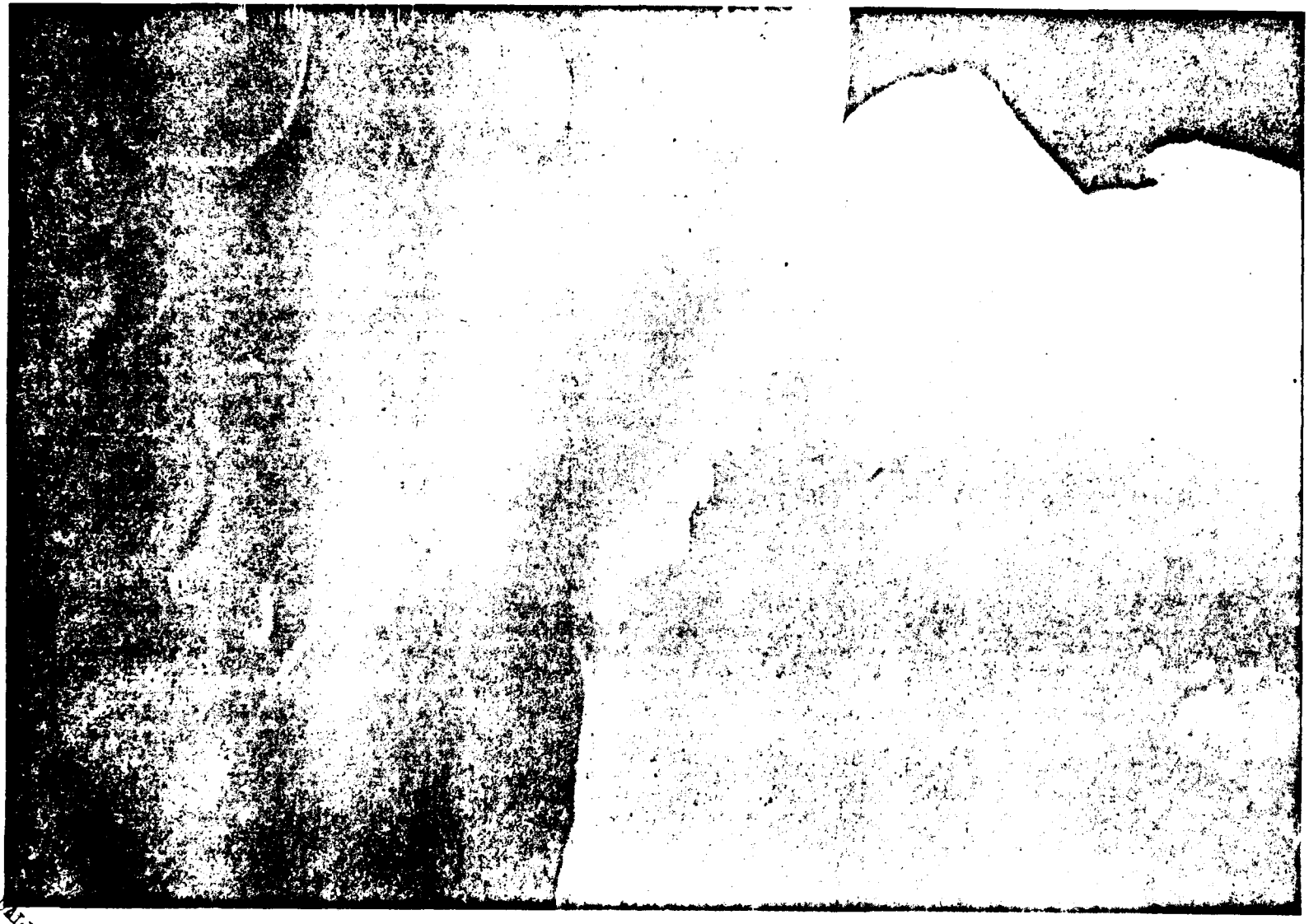

FIGURE 28 SCANNING ELECTRON PHOTOMICROGRAPHIC CLOSE-UP OF THE SPHERE DEPICTED IN FIGURE 27 SHOWING THE POINT OF CONNECTION BETWEEN SPHERE AND ROD

THIS PAGE IS BEST QUALITY PRACTICABLE
FROM COPY FURNISHED TO DDC

DAEDALEAN ASSOCIATES, Inc.

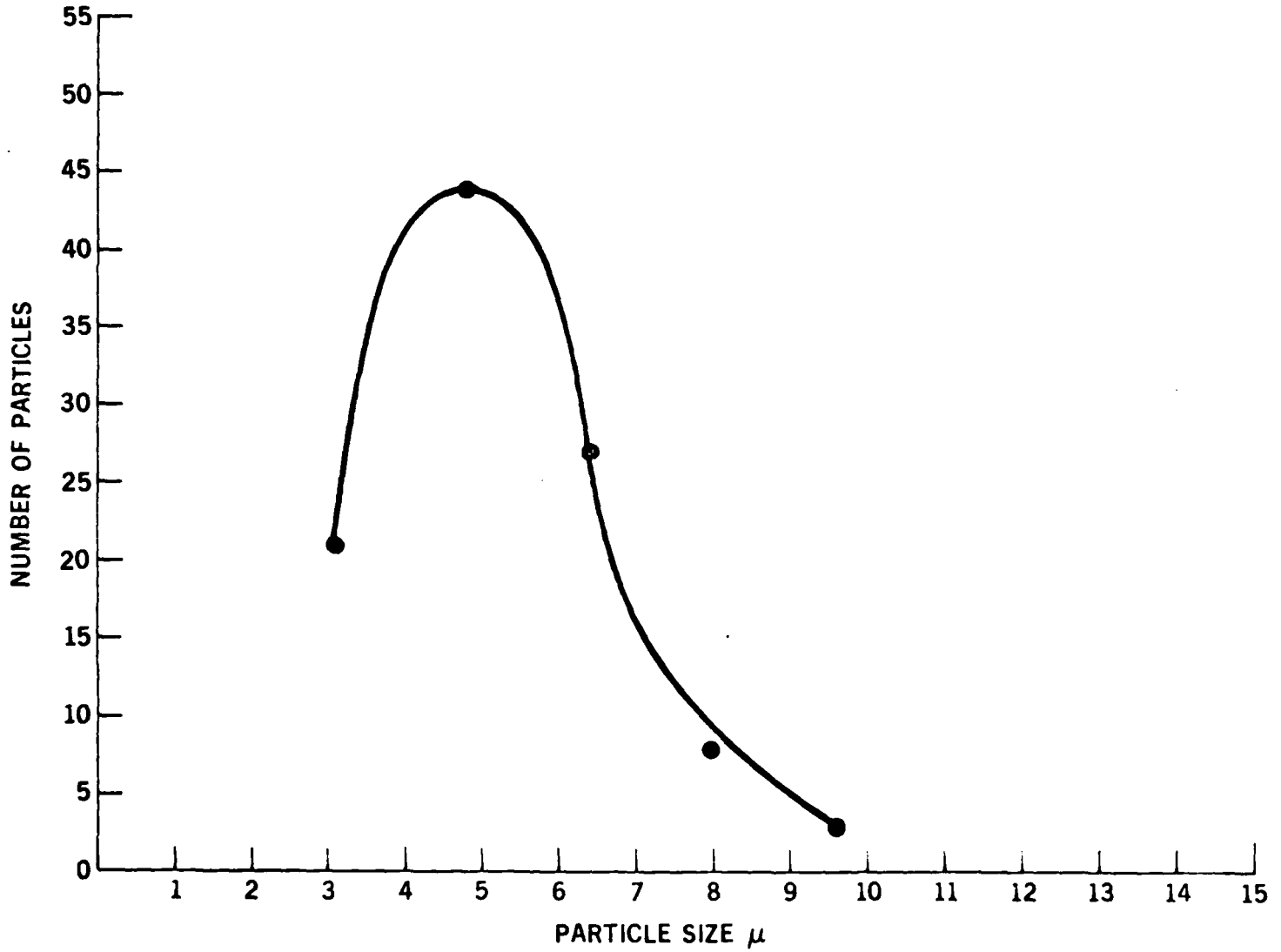

FIGURE 29 PARTICLE SIZE DISTRIBUTION CURVE FOR NICKEL SPHERICAL PARTICLES GENERATED FROM EROSION IN DISTILLED WATER

FIGURE 30 SCANNING ELECTRON PHOTOMICROGRAPH OF AN 8μ NICKEL SPHERICAL PARTICLE GENERATED FROM EROSION IN DISTILLED WATER

THIS PAGE IS BEST QUALITY PRACTICABLE
FROM COPY FURNISHED TO DDC

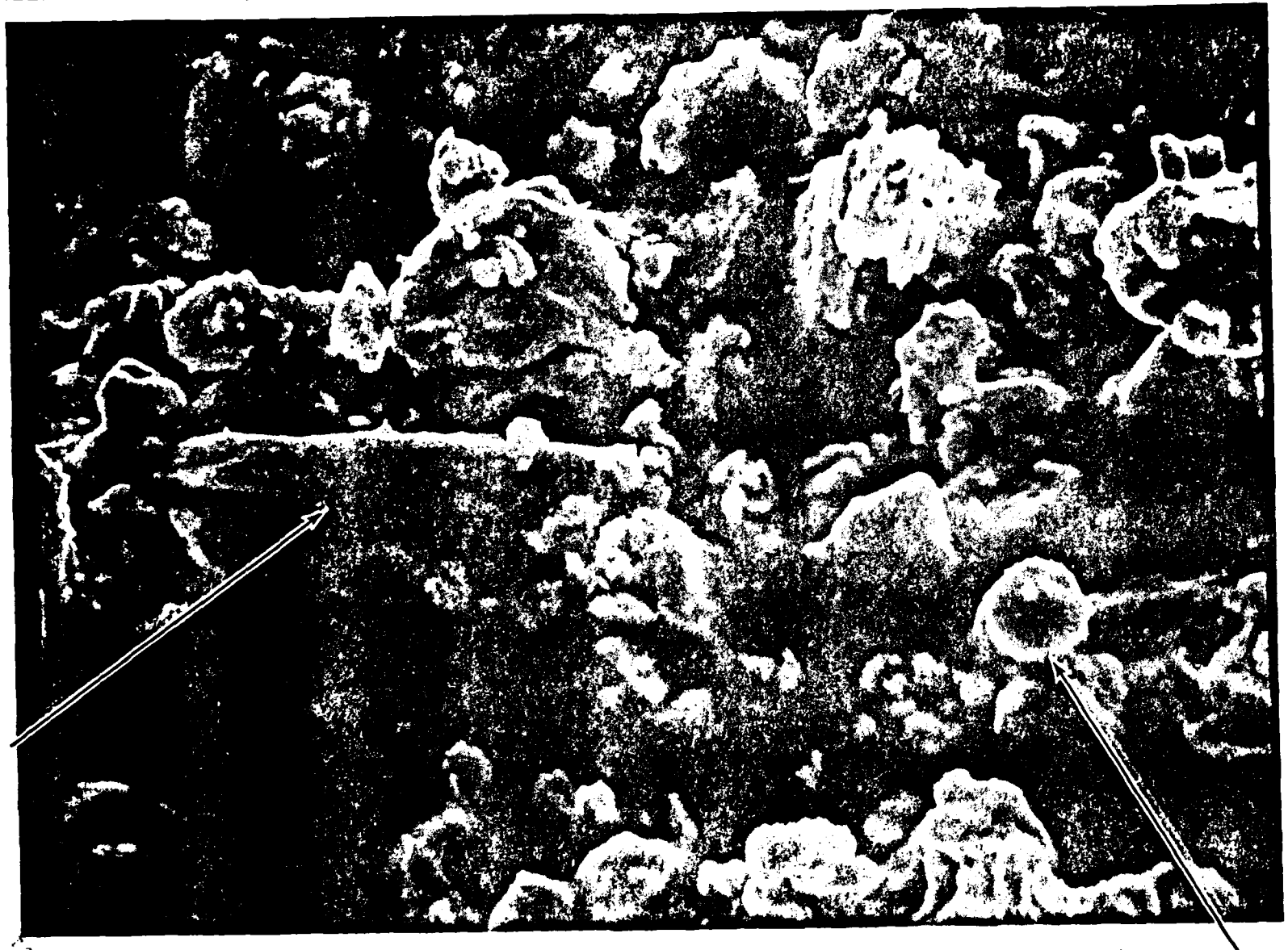

FIGURE 31 SCANNING ELECTRON PHOTOMICROGRAPH OF A 28μ LONG, 6μ DIAMETER NICKEL ROD IN CLOSE PROXIMITY TO A 7μ NICKEL SPHEROID

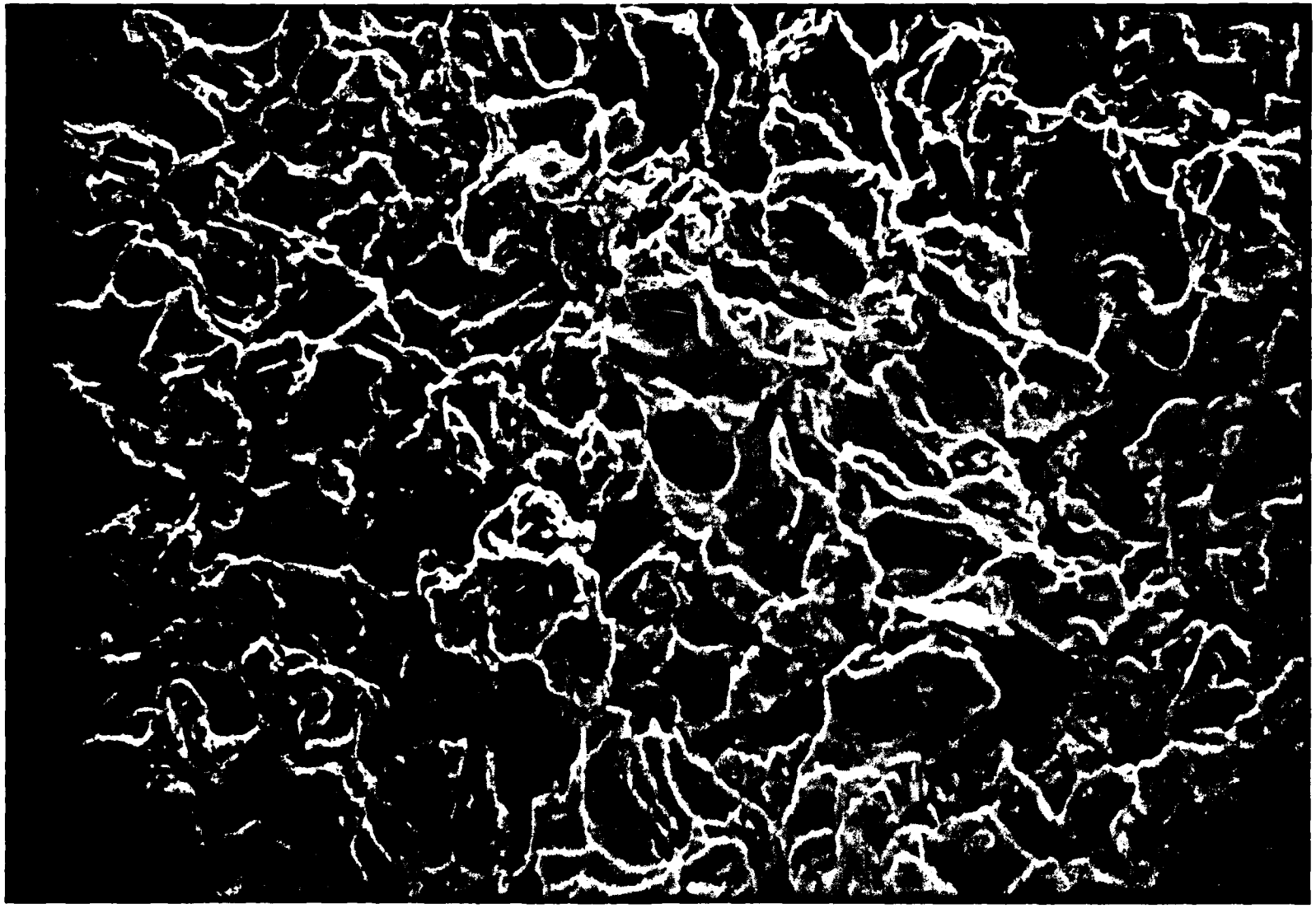

THIS PAGE IS BEST QUALITY PRACTICABLE
FROM COPY FURNISHED TO DDC

FIGURE 32 SCANNING ELECTRON PHOTOMICROGRAPH OF THE ERODED FACE OF THE NICKEL VIBRATORY BUTTON SHOWING PLASTIC DEFORMATION

BEST AVAILABLE COPY
FURNISHED TO DDC

FIGURE 33 SCANNING ELECTRON PHOTOMICROGRAPHIC CLOSE-UP OF THE NICKEL VIBRATORY BUTTON FROM FIGURE 32 SHOWING A 9 μ CONCAVE CRATOR